MECHANICAL DESIGN AND FABRICATION OF STRETCHABLE CONDUCTORS WITH APPLICATIONS TO ANTENNAS

by

XingJie Jiang
M.Sc. (Physics), University of New Brunswick, 2007

THESIS SUBMITTED IN PARTIAL FULFILLMENT OF
THE REQUIREMENTS FOR THE DEGREE OF

MASTER OF APPLIED SCIENCE

in the
School of Engineering Science
Faculty of Applied Sciences

SIMON FRASER UNIVERSITY

Spring 2012

APPROVAL

Name: **XingJie Jiang**

Degree: **Master of Applied Science**

Title of Thesis: **MECHANICAL DESIGN AND FABRICATION OF STRETCHABLE CONDUCTORS WITH APPLICATIONS TO ANTENNAS**

Examining Committee:

Chair: **Dr. Andrew Rawicz, P. Eng**
Professor, School of Engineering Science

Dr. Carlo Menon, P.Eng
Senior Supervisor
Assistant Professor, School of Engineering Science

Dr. Rodney Vaughan
Supervisor
Professor, School of Engineering Science

Dr. Ash M. Parameswaran, P.Eng
Supervisor
Professor, School of Engineering Science

Dr. Behraad Bahreyni, P.Eng
Internal Examiner
Assistant Professor, School of Engineering Science

Date Defended: 23 February 2012

Declaration of
Partial Copyright Licence

ABSTRACT

This thesis focuses on the mechanical investigation, design and fabrication of stretchable conductors with applications to antennas. Specifically, a stretchable patch antenna (SPA) whose frequency is tuned by a planar dielectric elastomer actuator (DEA) is proposed and analysed. This mechanically reconfigurable antenna system has a configuration resembling a pre-stretched silicone belt embedded with conductive liquid metal, which forms the patch antenna, and it has conductive electrodes, which form the DEA. Actuation of the DEA varies the side length of the patch antenna, and, as a result, its resonance frequency. Design and fabrication steps of this system are presented. Measurement results for deformation, resonance frequency variation and efficiency of the patch antenna are also presented.

Keywords: stretchable patch antenna; SPA; reconfigurable antenna; dielectric elastomer actuator; DEA

ACKNOWLEDGEMENTS

It is my pleasure to thank the many people who supported me during my study at Simon Fraser University. I am heartily thankful to my supervisor, Dr. Carlo Menon, whose encouragement, guidance, and support throughout my research enabled me to develop this subject.

Deep thanks to Dr. Shahrzad J. Mazlouman for her help, cooperation and suggestions on all aspects of the antenna research.

Many thanks also to Dr. Rodney Vaughan for his ideas on the application of combining both DEA with reconfigurable antennas as well as his instructive comments on this project and thesis. Special thanks also for his kind help on allowing us to use his equipments for antenna measurements. Without his help, the measurements of the antenna could not have been completed.

I want to thank Dr. Ash M. Parameswaran who also provided generous help on my DEA research by allowing us to utilize his equipment in his lab for our research.

I also want to thank Dr. Michael Sjoerdsma and my colleague, Jeff Krahn, who helped me on my thesis writing. Their advices are very valuable to me.

I want to give many thanks to all of my colleagues; their suggestions, help and encouragement were very important to me during my studies.

I also want to thank the Natural Sciences and Engineering Research Council of Canada (NSERC) and CMC Microsystems for the financial support through my supervisor’s grants.

I wish to express my love and gratitude to my family and my beloved loyal friend and partner of my life, Hui Lu. Without her patient assistance and encouragement, I could not have finished this thesis!

TABLE OF CONTENTS

Approval ii
Abstract iii
Acknowledgements iv
Table of Contents vi
List of Figures viii
List of Tables x
List of Acronyms xi

1: Introduction 1
1.1 Reconfigurable stretchable antenna 1
1.2 Antenna actuator 2
1.3 Objectives 2
1.4 Structure of this thesis 3

2: Literature review 4
2.1 Stretchable antennas 4
2.2 Dielectric Elastomer Actuator 5

3: Introduction of the stretchable patch antenna system using a dielectric elastomer actuator 8
3.1 The configuration of the stretchable patch antenna system using a dielectric elastomer actuator 8
3.2 SPA and the groundplane 10
3.3 The actuator 12
3.4 Summary 13

4: Manufacturing the stretchable antennas 14
4.1 Manufacturing the micro-channel in TC5005 substrate 14
4.2 Stretchable Patch Antennas 18
4.2.1 The stretchable patch antenna with an isolating layer inside 19
4.2.2 Removing the isolating layer from the stretchable patch antenna 27
4.3 Summary 31

5: Dielectric elastomer actuator 32
5.1 Analysis of the dielectric elastomer actuator 32
5.1.1 The electrostatic stress of the dielectric elastomer actuator 32
5.1.2 Analytical simulations of the planar dielectric elastomer actuator 34
5.1.3 An alternative method to simulate the planar dielectric elastomer actuator 37
5.2 Fabrication of the dielectric elastomer actuator 38

5.3 Summary....41

6: Finite Element analysis of the stretchable patch antenna system using dielectric elastomer actuator....42

6.1 Finite element model....42

6.2 Optimizing the dielectric elastomer actuator for the stretchable patch antenna system....46

6.3 Comparison of the experimental results and simulations....53

6.4 Summary....54

7: The prototype of the strEtchable patch antenna system using dielectric elastomer actuator....55

7.1 The first prototype of the stretchable patch antenna system using dielectric elastomer actuator....55

7.2 The compacted prototype of the stretchable patch antenna system using dielectric elastomer actuator....57

7.3 Summary....58

8: Conclusion and future work....59

8.1 Conclusion....59

8.2 Future work....60

Appendix A....61

Reference List....62

LIST OF FIGURES

Figure 3-1: Schematic diagram of the SPA-DEA system 9

Figure 3-2: The top and bottom views of the SPA-DEA system. 10

Figure 3-3: The effect of the groundplane side size on the S_{11} of the antenna. 12

Figure 4-1: Top view of the PMMA mold 15

Figure 4-2: Manufacturing process of the microchannel in the TC5005 substrate: (a) Uncured TC5005 in the mold; (b) Sealing the microchannel with uncured TC5005; (c) inject Galinstan into the channel 16

Figure 4-3: (a) Fabricated microchannel in the TC5005 substrate; (b) A leaking microchannel in TC5005 substrate 17

Figure 4-4: The microchannel in the TC5005 substrate (a) twisted, (b) folded, and (c) stretched 18

Figure 4-5: PMMA Mold for the SPA substrate. 19

Figure 4-6: The top elastomer layer collapsing on the bottom elastomer layer 20

Figure 4-7: Manufacturing process of the SPA with an isolating layer inside: (a) Prepared PMMA mold (b) TC5005 substrate cast on the mold (c) the substrate placed inversely (d) prepared top layer (placed the PE film) (e) spread the uncured TC5005 (f) bonded top layer and the bottom layer (g) inject the Galinstan 21

Figure 4-8: SPA is folded, twisted, and stretched. 22

Figure 4-9: Bubbles are stuck in between of the TC5005 layers 23

Figure 4-10: Update manufacturing process of the SPA with an isolating layer: (a) the cured TC5005 sheet (b) PE film on top of the first layer (c) spread uncured TC5005 (d) inject the Galinstan 24

Figure 4-11: (a) Satimo StarLab^{TM} anechoic chamber. (b) Results for the radiation efficiency of the SPA (an isolating layer inside) for various patch side lengths [8]. 26

Figure 4-12: Manufacturing steps of the SPA: (a) placed flat sheet of cured TC5005 (b) placed PE film and PMMA block (c) spread uncured TC5005 (d) removed the PMMA block and PE film (top view) (e)spread again uncured TC5005 to seal the channel (f) injected liquid metal 29

Figure 4-13: Results for the radiation efficiency of the SPA without an isolating layer for various patch side lengths 30

Figure 5-1: The schematic diagram of the cross section of the DEA. 33

Figure 5-2: The schematic diagram of the planar DEA. 35

Figure 5-3: Fabrication steps of the DEA. 40

Figure 6-1: (a) Schematic diagram of the DEA; (b) Parameters used to describe the three DEA states, namely (1) relaxed, (2) mechanically pre-stretched, and (3) electrically activated. 44

Figure 6-2: The algorithm diagram for simulations. 45

Figure 6-3: $\Delta x/x_p$ of the x component pre-strain of the DEA (E=10V/µm). 48

Figure 6-4: $\Delta x/x_p$ to C (S_x = 25%, S_y = 100%, E = 10V/µm). 49

Figure 6-5: Displacement of the x axis versus prestretched DEA Area (A_p). (a) Zoomed out view; (b) Zoomed in view highlighting the requested maximum deformation the DEA should provide. (S_x = 25%, S_y = 100%, E = 10V/µm, C = 30%). 52

Figure 6-6: Strain of the patch antenna along the x axis for different values of the imposed electric field. 53

Figure 6-7: Variations of the measured S_{11} of the antenna system for various patch side lengths that can be attained using the DEA small belt system. 54

Figure 7-1: The first prototype of the SPA-DEA system 56

Figure 7-2: The final prototype of SPA-DEA system 58

LIST OF TABLES

Table 1-1: List of EAP types and their properties.....7
Table 6-1: Range and step size of the FEM parameters.....47

LIST OF ACRONYMS

DEA	dielectric elastomer actuator
EAP	electro-active polymer
FEM	finite element method
PDMS	polydimethylsiloxane
PE	polyethylene
PMMA	polymethylmethacrylate
SPA	stretchable patch antenna

1: INTRODUCTION

Bendable and stretchable electronic devices have drawn the attention of engineers because of their soft features and promising performance [1]. In this work, mechanical investigations of a reconfigurable and stretchable antenna are performed. In addition, a polymer-based actuating system to tune the strain of the antenna is proposed and optimized.

1.1 Reconfigurable stretchable antenna

To adapt to changing environments and system requirements, antennas need to be reconfigurable. Reconfigurable antennas are currently applied to portable wireless devices, because they can improve signal-to-noise ratio or reconfigure radiation parameters to redirect transmitted power for saving battery life [2].

Incorporating actuators to reconfigure the physical structure of the antennas allows the antennas to obtain different configurations. Because mechanically reconfigurable antennas use advances in smart materials and very large scale integration, they are more likely to be used in industry. Recently, researchers have discovered light-weight, bendable, and stretchable antennas that are fabricated by injecting liquid metal into a silicone elastomer [3]-[7]. This new type of stretchable antenna could be a new generation of reconfigurable antenna.

Although, cooper antennas are highly efficient, the material fatigue of copper will not allow these antennas to be repeatedly bent. Thin foil may be used for bending, but is not stretchable and cannot smoothly change its surface area. However, stretchable antennas do not have such problems because they are fabricated out of silicone elastomer injected with liquid metal.

Only a few stretchable antennas have been reported in literature; a newly developed stretchable patch antenna (SPA) was fabricated in order to add this area [8].

1.2 Antenna actuator

The ideal actuator should be fabricated from the same flexible and stretchable material as the SPA in order to be used seamlessly in the same applications. A dielectric elastomer actuator (DEA) was firstly implemented on the SPA, which is called the SPA-DEA system. This DEA was selected because it was also fabricated using silicone elastomer [9]-[18]. The DEA has light-weight, low-cost, easy-to-manufacture characteristics [9]-[18]. The DEA was electrically activated by using a voltage amplifier (EMCO Q101), and consumed a maximum of 0.5 Watt [18].

1.3 Objectives

In order to achieve a SPA, the following objectives were defined:

Objective 1: Propose an innovative SPA-DEA configuration

Objective 2: Propose and test a manufacturing procedure to fabricate an SPA.

Objective 3: Fabricate a DEA

Objective 4: Optimize the mechanical design of the SPA-DEA configuration

Objective 5: Characterise the performance of the SPA-DEA system

1.4 Structure of this thesis

In this thesis, Chapter 2 is the literature review of the stretchable antenna and DEA. Chapter 3 proposes configurations of the SPA-DEA system while Chapters 4 and 5 present a detailed manufacturing process for stretchable antennas and DEAs respectively. In addition, Chapter 5 also introduces related basic electromechanical concepts of the planar DEA and presents our analysis methods. Chapter 6 introduces the finite element model that was used for optimizing the design parameters of the tunable antenna and for improving the efficiency of the SPA-DEA system. Experimental results and a comparison with simulations using finite element method (FEM) are shown in Chapter 6 while chapter 7 shows our prototype system and the final chapter offers conclusions based on this work.

2: LITERATURE REVIEW

2.1 Stretchable antennas

A stretchable, frequency-reconfigurable monopole antenna was fabricated by injecting a liquid metal (Galinstan) into a micro-channel of a polydimethylsiloxane (PDMS) substrate [7]. It was shown that the resonant frequency of the liquid metal wire antenna can be tuned by stretching the substrate, thereby altering the effective length of the antenna. Similarly, flexible loop and cone antennas were implemented [19]. Although not designed for a reconfigurable antenna, some frequency and pattern variation due to stretching were reported for the loop antenna [19]. The measured mechanical strain for these flexible antennas is limited to 40%, because their rigid feeding mechanism will easily damage them when the strain exceeds 40% [1].

In addition, when the antenna was twisted or folded, the rigid connections also have an adverse influence on measurements [1]. Later, a hybrid substrate for flexible antennas was presented in order to increase the strain up to 120% by incorporating a more elastic substrate around the rigid components while maintaining the PDMS substrate [20]. However, the rigid feed connections are still reported to decrease the durability of the flexible antennas [1], [19]. For our SPA, in order to reduce the limitation of the rigid feed connection, we alternatively used a coupled feeding mechanism [21], [22], which allowed the patch antenna to stretch freely while the feeding system is fixed.

In addition, in previous works, the PDMS was used for the substrate of the antenna, and it could only provide a maximum strain of 140% [23]. In our study, we used more stretchable material, TC5005 silicone (BJB Enterprises) [24], for our substrate. This new SPA then can realize 300% strain along one direction [8].

2.2 Dielectric Elastomer Actuator

In 1880, Roentgen investigated the first electro-active polymer (EAP). He observed natural rubber was changed in shape when a large electrical field was applied crossly. Today, a wide number of EAPs have been discovered, and various materials were studied for EAPs. EAPs can be broadly categorised into two classifications based on their actuation methods: ionic and field-activated. The ionic polymer includes ionic polymer–metal composites (IPMC), ionic gels, carbon nano-tubes, and conductive polymers (CPs). Field-activated polymers on the other hand include those made from ferroelectric polymers, polymer electrets, electrostrictive polymers, and dielectric elastomers (DEs).

The actuator used for our system was a dielectric elastomer actuator (DEA) in a silicone (TC5005) substrate. From Table1-1, the ionic EAPs usually have high maximum strain and low maximum stress, and, in contrast, field-activated polymers have a relatively low strain, but the stress is higher. The DEA in a silicone substrate is a kind of EAP that can balance these two characteristics [9]-[18], [25]. It can be fabricated out of the same silicone, TC5005, which is used for the SPA, which is more convenient for manufacturing.

A DEA can be considered as a DC parallel plate capacitor with two electrodes which are attracted by an electrostatic force that causes a planar expansion of the elastic dielectric material [9]. Therefore, selecting appropriate materials for the electrodes and dielectrics is a key factor for improving the ratio of converting electrical energy to mechanical energy. Because the elastic dielectric must accommodate a large mechanical strain, a good compliant electrode material for DEAs should have a lower stiffness than the dielectric layer and must maintain good conductivity at large deformation. Commonly used materials for electrodes include metallic paints, carbon grease, graphite and carbon powder, etc [10]. Carbon grease electrodes are commonly used because they maintain good conductivity at high strain and provide good adhesion to most DE materials [10], [11]. Dry carbon powders also have similar benefits to those found with carbon grease, and they are even easier to handle. However, the materials they can be adhered to are selective. Fortunately, carbon powder has good adhesion to TC5005 silicone. A comparison of electrode materials was investigated by Carpi *et al*. in 2003 [10], [11].

To investigate the performance of a DEA, the characteristics of the dielectric should be studied first. Presently, the most used dielectric materials are categorized into two groups: acrylics and silicones [10], [12], [14], [18]. These devices have also been modeled using linear assumptions as well as modeled as non linear systems [10], [13]. For our DEA device, we used TC5005 silicone as the base. The maximum strain of TC5005 for our application was 100%±10% which still has linear behavior if we looked at the force-displacement diagram in

[18]. Therefore, we considered the TC5005 silicone that is used for fabricating SPA and DEA to be a linear elastomer. In addition, because pre-strain significantly improves the performance of DEAs [14], a finite element model was built to discover the best pre-strain for our system.

Table 1-1: List of EAP types and their properties

Type	Maximum strain (%)	Maximum pressure (MPa)	Maximum efficiency (%)	Ref.
Delectric elastomer (acrylic)	380	7.2	60-80	[25], [26], [28]
Delectric elastomer (silicone)	32	1.36	90	[25]
Electrostrictive polymer	4.3	43	~80	[25]
Electrostatic device	50	0.03	>90	[25], [27], [28]
Piezoelectric polymer	0.1	4.8	-	[25]
Shape memory alloy	>5	>200	<10	[25]
Conducting Polymer	10	450	<5	[25], [27]
Ionic gel	>40	0.3	30	[25]
Natural muscle	>40	0.35	>35	[25]

3: INTRODUCTION OF THE STRETCHABLE PATCH ANTENNA SYSTEM USING A DIELECTRIC ELASTOMER ACTUATOR

3.1 The configuration of the stretchable patch antenna system using a dielectric elastomer actuator

The stretchable patch antenna system using a dielectric elastomer actuator (SPA-DEA system) is displaced in Figure 3.1. The SPA-DEA system works on a belt system with the belt embedded with an SPA on the upper segment and a planar DEA on the lower segment. The DEA and SPA were fabricated using the same silicone substrate, TC5005 (BJB, USA [24]) and were connected by an inextensible cloth. The belt was pre-stretched using two fixed rollers (Figure 3-1) and kept at a fixed distance apart by a rigid element (copper clad board), which also served as a groundplane for the antenna. A plastic spacer inserted between the SPA and the groundplane was used to maintain constant spacing while stretching the SPA. When the DEA was actuated by applying a voltage, it expanded laterally. The inextensible material (cloth) transferred this displacement and caused the SPA to contract. The deformation of the DEA is always contrary to the deformation of the SPA in this case.

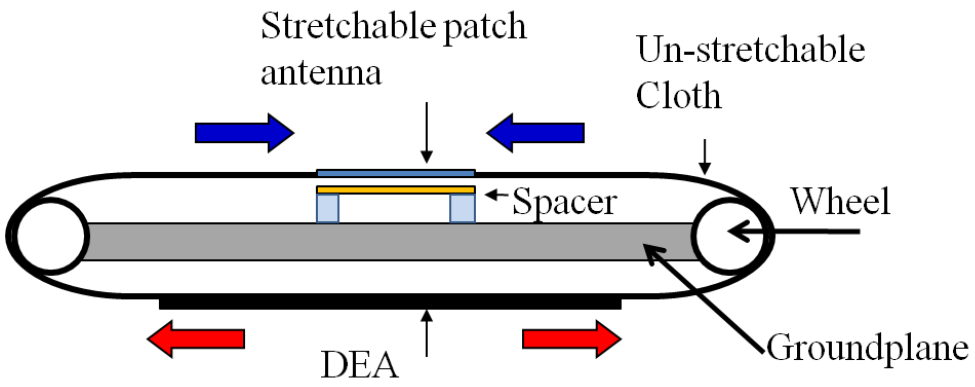

Figure 3-1: Schematic diagram of the SPA-DEA system

Figure 3-2 shows both the top and bottom views of the proposed system. The top view (figure 3-2 a) shows the SPA bonded to the inextensible cloth. The cloth was fully attached along two opposing edges of the SPA in order to stretch the SPA evenly and ensure that the SPA is not twisted. The bottom view (Figure 3-2 b) shows that the DEA was prestretched and constrained vertically and only could expand horizontally. As discussed later in Chapter 5, the un-stretchable cloth was not fully attached along two sides of the DEA because the length of the connection between them contributes to the efficiency of the DEA.

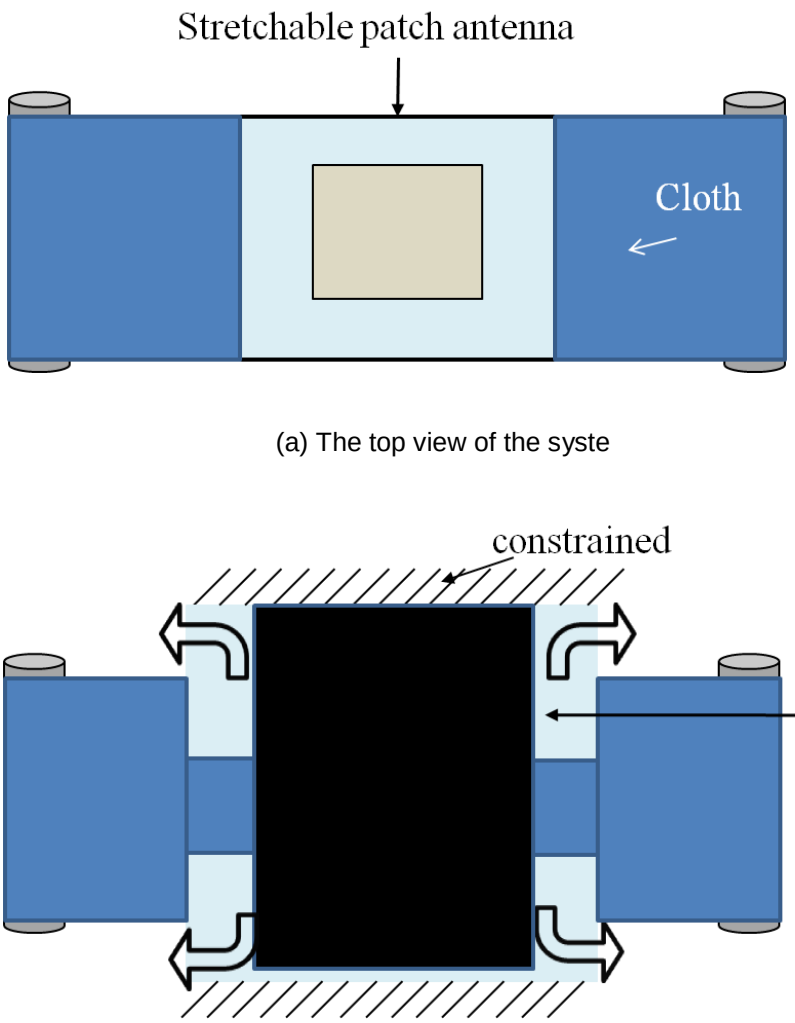

(a) The top view of the syste

(b) The bottom view of the system

Figure 3-2: The top and bottom views of the SPA-DEA system.

3.2 SPA and the groundplane

In order to operate near the Universal Mobile Telecommunications System (UMTS) frequency bands [29], the side length of the patch antenna was selected to vary between 40mm-53mm. This selection also enabled us to perform

measurements with the tools available in our laboratory, which are calibrated for these bands.

For an SPA, an infinite groundplane is always ideal but, for real applications, the groundplane had finite dimensions for real applications (Figure 3-1). Simulation performed by Dr. Mazlouman using CST^{TM} Microwave Studio confirmed that the finite groundplane does not have a significant effect on the performance of the antenna, unless the stretched patch antenna sides get close to the edges of the groundplane. If the sides of the stretched patch antenna are too close to the edges of the ground plane, the radiation due to the groundplane edges begins to affect the performance of the antenna. This effect was simulated by Dr. Mazlouman for various square groundplane side dimensions by considering a deformed patch antenna with 53 mm side length. Figure 3-3 shows the CST^{TM} numerical simulation results for measuring of the input port voltage reflection coefficient, S_{11}, from the antenna. As shown in Figure 3-3, the frequency of operation of the antenna starts detuning when the groundplane side gets smaller than 70 mm. Therefore, a 70mm square groundplane was chosen.

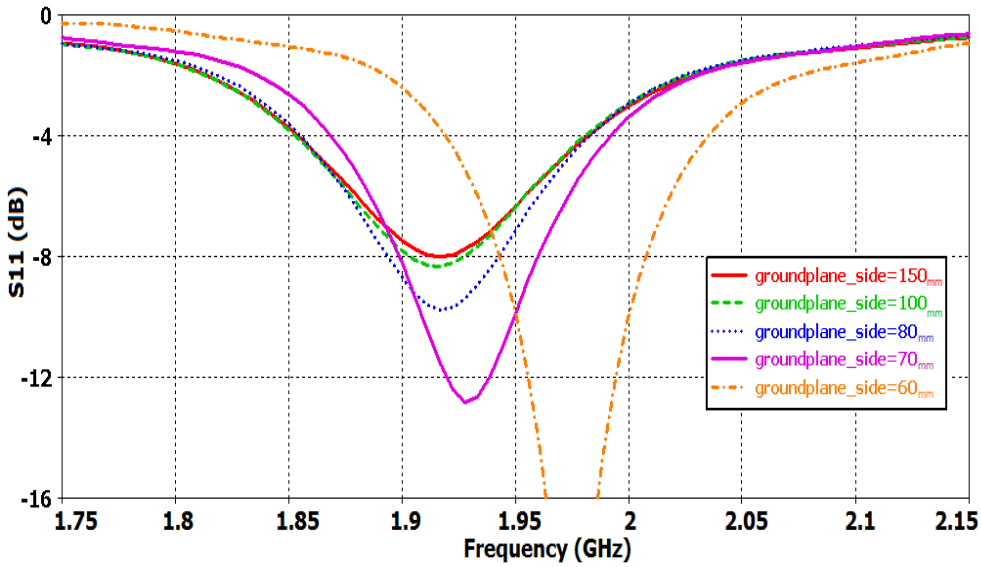

Figure 3-3: The effect of the groundplane side size on the S_{11} of the antenna.

3.3 The actuator

In the proposed configuration, as previously seen in Figure 3-1, the DEA is used to control the side length of the SPA. It is desirable to design the DEA such that its size is minimized in order to obtain an overall compact system. Note that the effective deformations of the DEA are highly influenced by the amount of its initial pre-stretching and the imposed boundary constraints. A finite element model of the system was therefore developed to investigate the effect of these parameters, which is discussed in Chapter 6.

3.4 Summary

In this chapter, objective 1 was accomplished. An innovative SPA-DEA configuration was proposed which is able to adjust the frequency of the SPA. The need to varying the side length of the SPA from 40 mm to 53 mm to tune the antenna frequency was given. The dimensions of the groundplane for the SPA were selected as 70 mm×70 mm. In addition, in order to ensure the system was compact and further improve the efficiency of the antenna, the DEA needed simulations.

4: MANUFACTURING THE STRETCHABLE ANTENNAS

This chapter demonstrates the micro-channel manufactured in the TC5005 substrate as well as the SPA with and without an inner isolating layer. By developing these three prototypes, the method of manufacturing the SPA was developed and gradually improved. The SPA without an isolating layer has been developed as the finial prototype, and it was embedded within the SPA-DEA system.

4.1 Manufacturing the micro-channel in TC5005 substrate

As mentioned previously, researchers have recently fabricated stretchable antennas or interconnections by injecting liquid alloy into an elastomer [3]-[7] that is mostly made out of polydimethylsiloxane (PDMS). The elongations of these antennas were only capable of reaching a maximum of 100% elongation. In our research, a more stretchable material, silicone TC5005, was used to increase the elongation. This silicone is comprised of three individual components: A, B, and C [24]. Component A is a type of silicone rubber base that belongs to the Organopolysiloxane chemical family [30]. Component B is a silicone catalyst that also belongs to the chemical family Organopolysiloxane [31]. Components A and B can be mixed at a weight ratio of 10:1 to form the most rigid TC5005 silicone. Component C is a Silicone-based fluid that belongs to the PDMS family and has short molecular chain, which is used to decrease the stiffness of the TC5005 [32]. Component C can be added to up to half the weight of A and B. Once the

amount of C exceeds this maximum amount, TC5005 will never cure (become a solid elastomer). In our study, we always preferred a more stretchable silicone as the substrate for the antenna therefore, component C was always added to the maximum amount.

In order to learn the fabrication methods of stretchable antennas, we first fabricated a microchannel in TC5005 substrate. Figure 4-1 below shows the top view of the mold made from polymethylmethacrylate (PMMA). A 60-watt CO_2 laser (VersaLASER® VLS3.60, 60W Laser Cartridge) cut a 70 mm×20 mm channel with a depth of 1mm, a narrow rectangular island with dimension of 65 mm×0.5 mm×1 mm as well as a cylindrical island 1 mm in diameter were left in the middle of the pool.

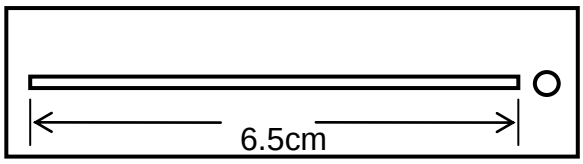

Figure 4-1: Top view of the PMMA mold

Figure 4-2 (a), (b), and (c) show a schematic of the manufacturing process of the microchannel in TC5005 substrate which was as follows: (a) First, we poured an uncured mixture of TC5005 into the PMMA mold and allowed it to cure for 16 hours. (b) The cured TC5005 substrate was demolded and placed cavity side up on a level table. Uncured TC5005 was used as a sealant by spreading it onto both sides of the micro channel. Then a second, thin flat, TC5005 silicone

layer was laid on top of the substrate. (c) After the sealant had cured we were left with a 65 mm×0.5 mm×1 mm chamber. This chamber was then injected with the liquid metal alloy Galinstan, creating a conductive microchannel in the TC5005 substrate.

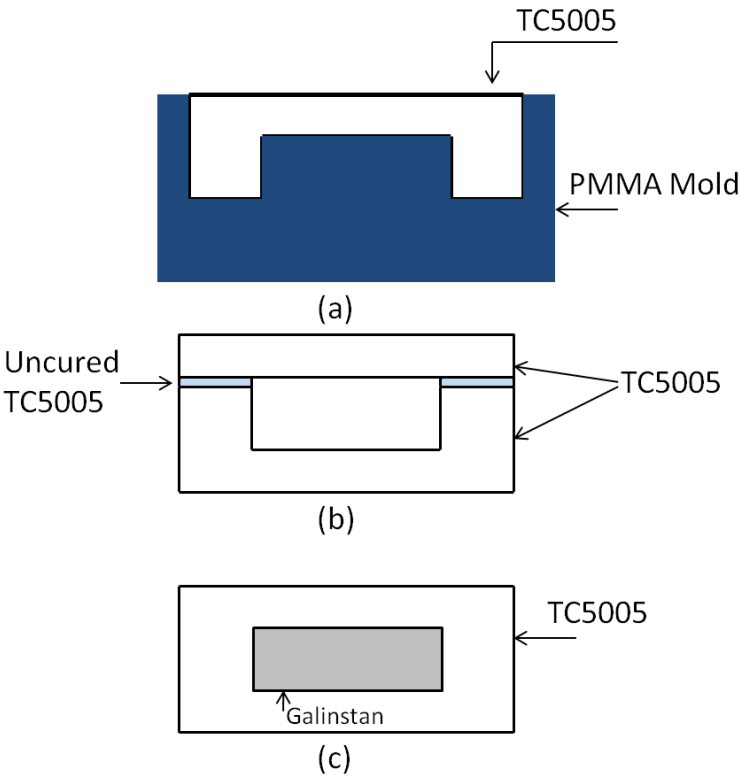

Figure 4-2: Manufacturing process of the microchannel in the TC5005 substrate: (a) Uncured TC5005 in the mold; (b) Sealing the microchannel with uncured TC5005; (c) inject Galinstan into the channel

In addition, it should be noted that the microchannel in the TC5005 substrate was self-sealing. Alongside the microchannel, a small round reservoir was also manufactured (Figure 4-3a). When Galinstan was injected to the microchannel, the needle was passed first through the reservoir and then on into the channel. When the needle had reached the bottom of channel, the Galinstan

was then injected, and the Galinstan repelled the air inside of the channel into the round reservoir. The air remained within the reservoir, keeping the Galinstan in the channel; therefore, we did not need to seal the sample again. The round reservoir also helps to see when the Galinstan within the microchannel is leaking from the sample. As shown in Figure 4-3b, once Galinstan begins to appear in the round reservoir this indicates that the air in the round reservoir has leaked out and the sample is no longer sealed.

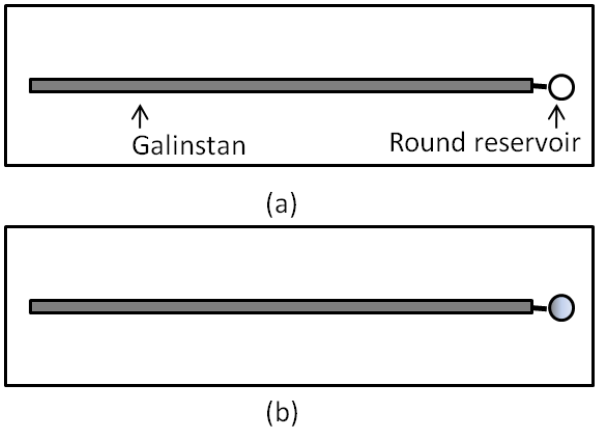

Figure 4-3: (a) Fabricated microchannel in the TC5005 substrate; (b) A leaking microchannel in TC5005 substrate

Figure 4-4 demonstrates that the microchannel in the TC5005 substrate can be twisted (Figure 4-4a), folded (Figure 4-4b) and stretched (Figure 4-4c).

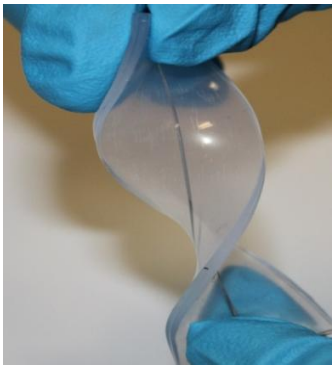

(a)

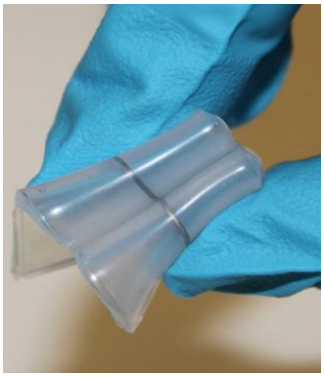

(b)

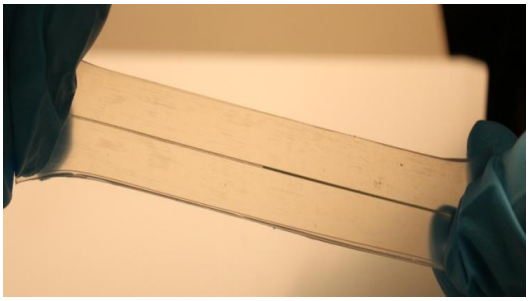

(c)

Figure 4-4: The microchannel in the TC5005 substrate (a) twisted, (b) folded, and (c) stretched

4.2 Stretchable Patch Antennas

After manufacturing the microchannel within the TC5005 substrate, our attention was then focused on developing the SPA. The stretchable patch antenna was made out of the TC5005 silicone substrate injected with liquid metal made with a similar manufacturing method to the Galinstan filled microchannel. In this section, two different types of SPA were developed, and their comparison is presented.

4.2.1 The stretchable patch antenna with an isolating layer inside

4.2.1.1 Manufacturing process

Similarly, to the microchannel described above, the mold for the patch antenna, as shown in Figure 4-5, was fabricated out of PMMA using the same laser cutter introduced in section 4.1. A 30 mm×30 mm×0.5 mm square island was left in the middle of the PMMA. After manufacturing the mold, TC5005 was cast within it.

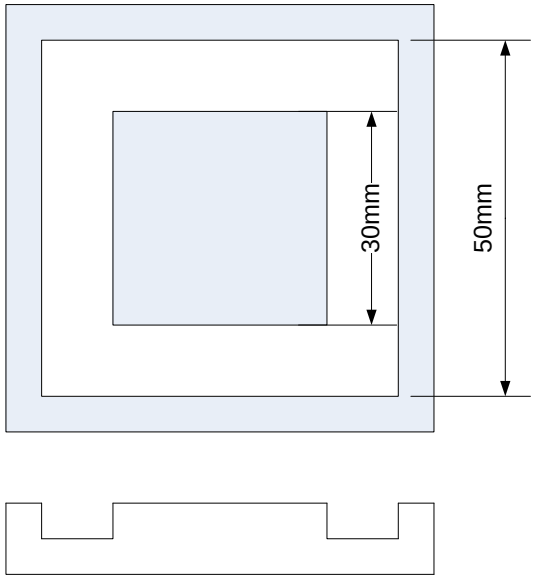

Figure 4-5: PMMA Mold for the SPA substrate.

After curing, the overall dimensions of the demolded silicone sheet were 50 mm×50 mm with a 30 mm×30 mm×0.5 mm reservoir for containing the Galinstan. To seal the silicone, uncured TC5005 was uniformly spread over a 50 mm×50 mm×1 mm flat sheet of TC5005 silicone. When the patterned layer was

placed on top of this flat sheet, because the TC5005 was softer and more stretchable than the PDMS, the top layer often collapsed and contacted the bottom layer, as shown in Figure 4-6. This caused the upper and lower portions of the two TC5005 sheets to often cure together and ruin the fabrication of the wide but thin reservoir.

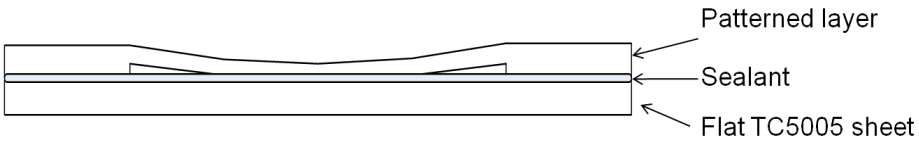

Figure 4-6: The top elastomer layer collapsing on the bottom elastomer layer

An isolating layer was required to stop the upper collapsed layer from bonding with the bottom layer. Because our experiments confirmed that TC5005 silicone does not bond with PE film (Figure 4-7), we used a 13.5 µm thick Polyethylene (PE) film as an isolating layer to separate the top and bottom layers.

Figure 4-7 shows the complete manufacturing process of the patch antenna with an isolating layer inside. In the first step, TC5005 was cast on a PMMA mold to create the patch antenna (Figure 4-7a). Secondly, uncured TC5005 was poured into the mold (Figure 4-7b). After curing, the TC5005 substrate was inverted (Figure 4-7c). Then, a 30 mm×30 mm×12.5 µm PE film [33] was placed on the patterned TC5005 (Figure 4-7d). In the fifth step, a

uniform sealant layer was sprayed over a 50 mm×50 mm×1 mm flat sheet of TC5005 (Figure4-7e). Subsequently, in the sixth step, the substrate with the PE film that was formed in the fourth step was placed on top of the flat sheet with a sealant layer (Figure 4-7f). In the final step, after curing, a square reservoir with an embedded PE film was inside the TC5005 substrate, and then the Galinstan was injected into the reservoir (Figure 4-7g).

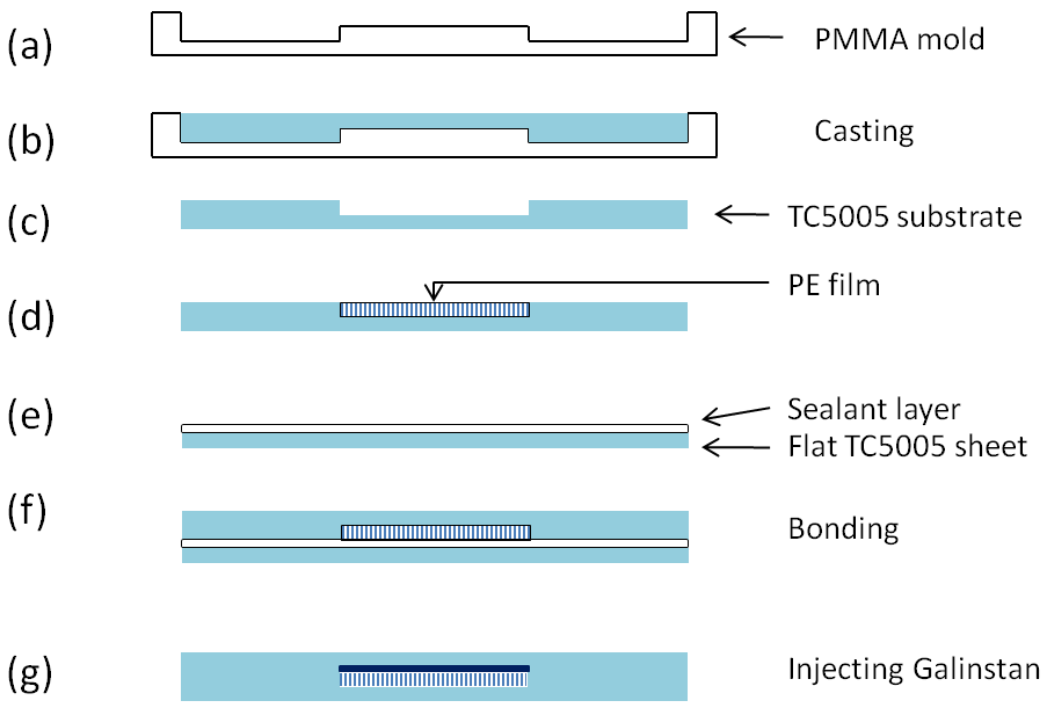

Figure 4-7: Manufacturing process of the SPA with an isolating layer inside: (a) Prepared PMMA mold (b) TC5005 substrate cast on the mold (c) the substrate placed inversely (d) prepared top layer (placed the PE film) (e) spread the uncured TC5005 (f) bonded top layer and the bottom layer (g) inject the Galinstan

Using this method, we first fabricated an SPA shown in Figure 4-8. The SPA can be folded (Figure 4-8a), twisted (Figure 4-8b), and stretched (Figure 4-8c)

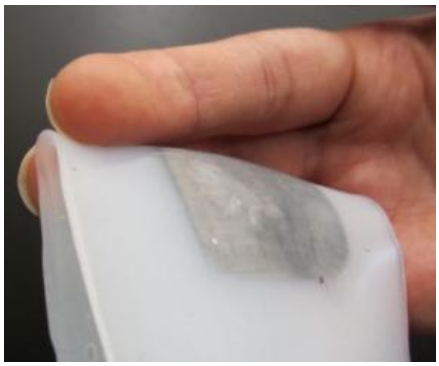

(a)

(b)

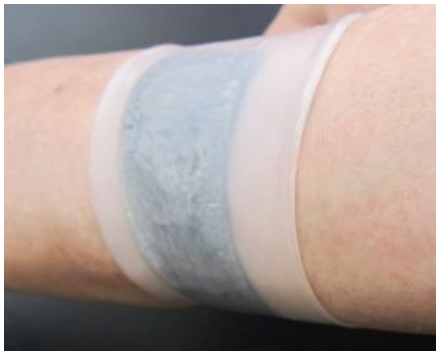

(c)

Figure 4-8: SPA is folded, twisted, and stretched.

After successfully manufacturing the first SPA, we continued to improve the fabrication method of the SPA. In the previous process, two TC5005 substrates were bonded by a layer of liquid sealant that was the uncured TC5005 (Figure 4-7f). However, bubbles in between the two cured layers were not released because of the narrow gap (Figure 4-9). Although bubbles trapped between the two substrates will not overly affect the sample, the bubbles trapped in the space reserved for the liquid metal were not negligible. Once the sealant

was cured, the voids caused by the air bubbles were filled with the liquid metal, which resulted in an irregular shape of the Galinstan.

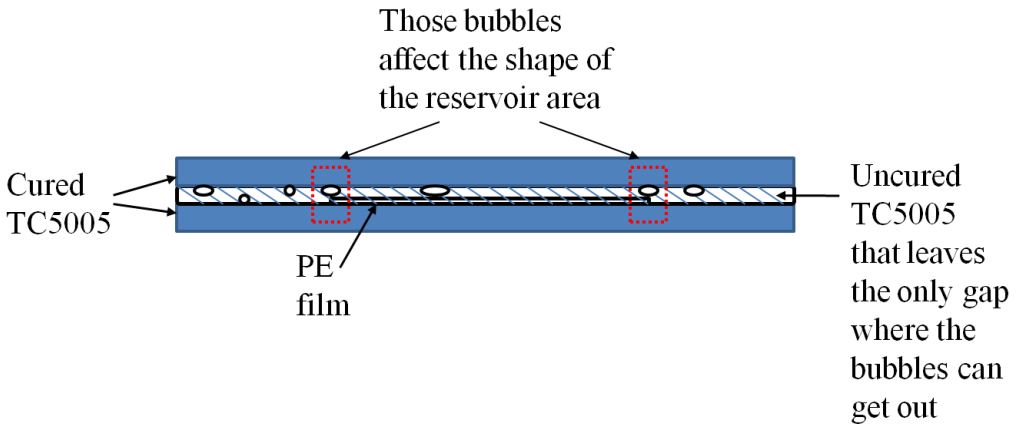

Figure 4-9: Bubbles are stuck in between of the TC5005 layers

A refined manufacturing process solved the bubble problem and increased the yield of good samples. At the same time, the fabrication steps were reduced from seven down to four steps, and the PMMA mold was made no longer necessary. The complete fabrication steps are shown in Figure 4-10 where, in the first step, a flat, cured TC5005 sheet was placed on a level table (Figure 4-10a). Secondly, a 30 mm×30 mm×12.5 μm PE film was laid on top of the TC5005 sheet (Figure 4-10b). In the third step, a layer of uncured TC5005, used as a sealant, was poured on top of a PE film and a TC5005 sheet (Figure 4-10c). After curing, the TC5005 substrate became a well sealed envelope (Figure 4-10d). Lastly, the liquid metal was injected into this envelope. Bubbles are often produced in the third step, but, because TC5005 takes 16-24 hours to fully cure

[24], bubbles in the uncured TC5005 layer easily escape from the wide open surface of TC5005 sheet during the curing time.

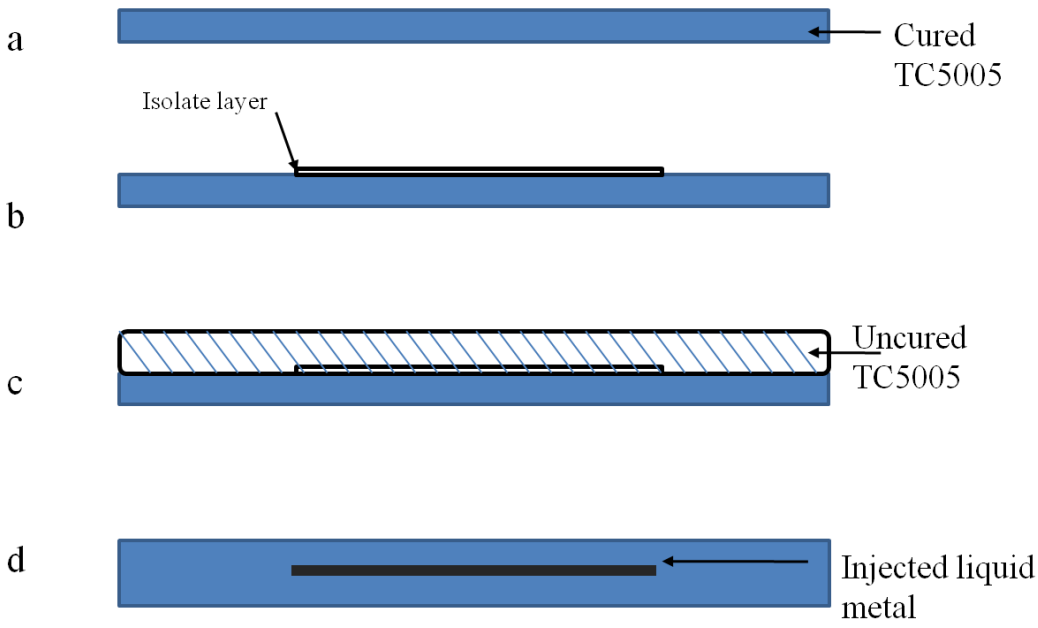

Figure 4-10: Update manufacturing process of the SPA with an isolating layer: (a) the cured TC5005 sheet (b) PE film on top of the first layer (c) spread uncured TC5005 (d) inject the Galinstan

4.2.1.2 Experimental measurements

The resonant frequency and radiation efficiency of this patch antenna was measured by Dr. Mazlouman using a vector network analyzer (Agilent) and a Satimo StarLab™ anechoic chamber. The chamber is represented in Figure 4-11a. Figure 4-11b shows the measurement results. In Figure 4-11b, the radiation efficiency of this antenna decreased when the patch antenna was stretched [8]. The relaxed patch antenna had 80% efficiency. When the patch antenna was stretched to 49mm in one dimension, the radiation efficiency of this antenna was

decreased to 75%; and when the patch antenna was stretched to 68 mm, the radiation efficiency of this antenna was decreased to 65%. One of reasons that caused this phenomenon might be the isolating layer (PE film) within the patch antenna. However, because the PE film is an un-stretchable material, when the SPA is stretched, the PE film is unable to deform with the SPA, which likely causes discontinuities in the Galinstan thus reducing the radiation efficiency of the SPA.

In order to improve the radiation efficiency of the SPA after stretching, we needed to employ a fabrication method that enabled removal of the isolating layer. The method used to achieve this is described in the next section.

.

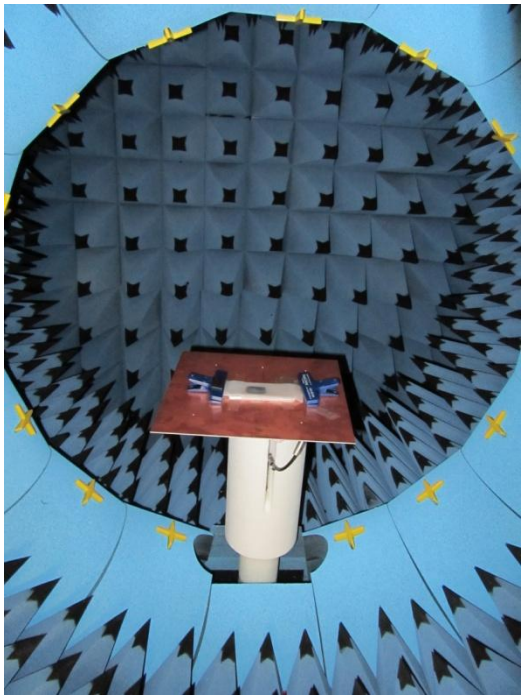

(a)

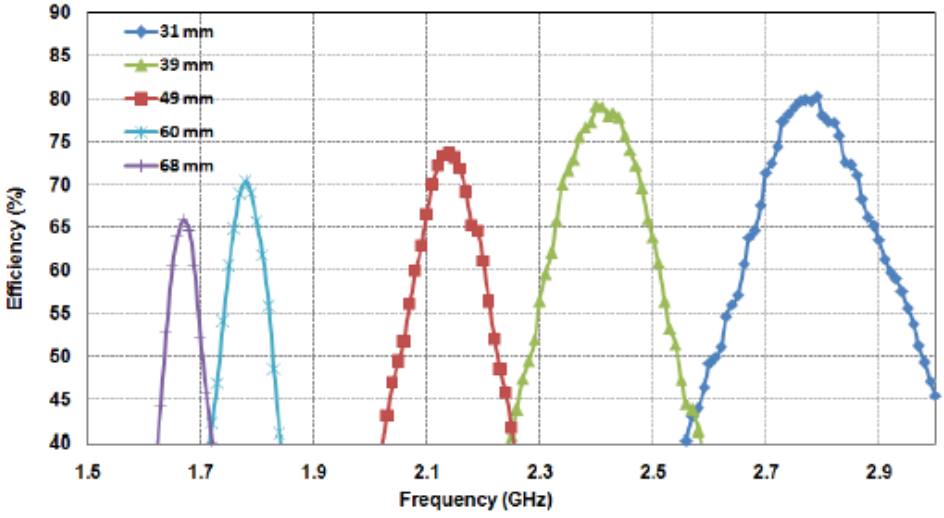

(b)

Figure 4-11: (a) Satimo StarLab™ anechoic chamber. (b) Results for the radiation efficiency of the SPA (an isolating layer inside) for various patch side lengths [8].

4.2.2 Removing the isolating layer from the stretchable patch antenna

An isolating layer was previously used to ensure a hollow cavity was available for injecting Galinstan into the SPA. Antenna efficiency measurements suggested that if the isolating layer could be removed from the SPA, the antenna may have much better performance than the previous version that included an isolating layer. This section demonstrated how the isolating layer is removed as well as the efficiency of the SPA using the new manufacturing method.

4.2.2.1 Manufacturing process

In order to remove the isolating layer inside of the SPA, we implemented a new manufacturing process. Figure 4-12 illustrates the six fabrication steps used to manufacture the SPA. In the first step (Figure 4-12a), a thin flat sheet of cured TC5005 silicone was placed on a levelled table. Subsequently, a 30 mm×30 mm×12.5 μm isolating PE film was placed on the top surface of the silicone sheet. A 20 mm×3 mm×2 mm PMMA block was then positioned next to the PE film (Figure 4-12b). In the third step, uncured TC5005 was spread over the top of the cured TC5005 sheet, PE film, and PMMA block. The fourth step consisted of two phases. In the first phase, the PMMA block was removed after the TC5005 top layer was cured. Removal of this small block formed an open channel (Figure 4-12d). In the second phase of this step, the PE film was removed via the channel created by the removal of the PMMA block. The PE film was selected to be flexible and foldable so that it could be folded into a strip and taken out from

the channel. The fifth step consisted of sealing the channel with uncured TC5005 (Figure 4-12e) in order to form a closed reservoir. In the last step, liquid metal (Galistan) was injected into the reservoir through a needle (Figure 4-12f). Note that the removal of the needle did not require additional sealing. Through this last step, a conductive liquid metal was trapped within a stretchable polymer envelope that formed the SPA.

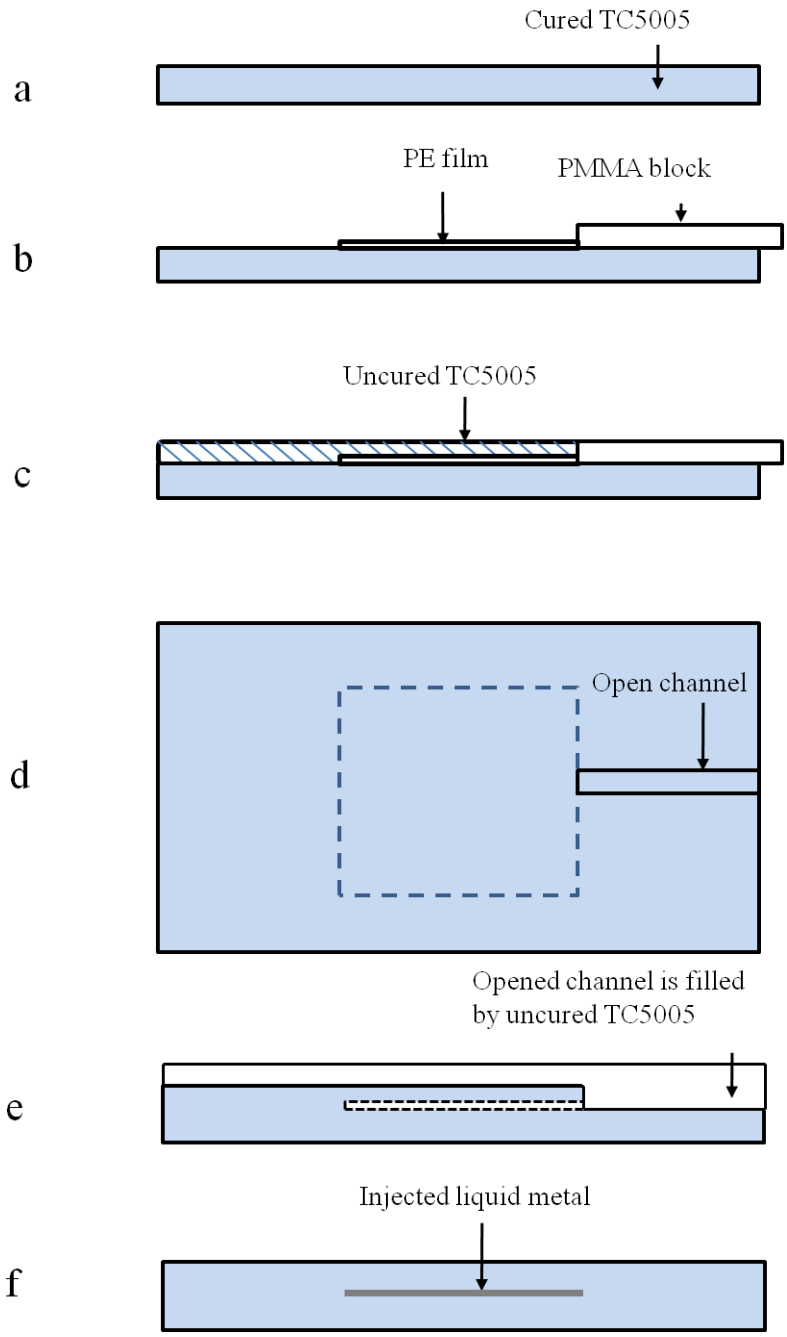

Figure 4-12: Manufacturing steps of the SPA: (a) placed flat sheet of cured TC5005 (b) placed PE film and PMMA block (c) spread uncured TC5005 (d) removed the PMMA block and PE film (top view) (e)spread again uncured TC5005 to seal the channel (f) injected liquid metal

4.2.2.2 Experimental Measurements

After the successfully removal of the isolating layer, this new SPA was embedded in the SPA-DEA system latterly. Figure 4-13 depicts the radiation efficiency of the antenna about various resonance frequencies and side lengths. The radiation efficiency was measured using a Satimo anechoic chamber and by Dr. Mazlouman. For all sweeping points, the radiation efficiency is always greater than 78%. This result shows that this new version of the SPA is better than the previous one with an isolating layer left inside since the radiation efficiency of the SPA with the isolating layer dropped from 80% to less than 75% within the side length range [39mm, 49mm] as shown previously in figure 4-11.

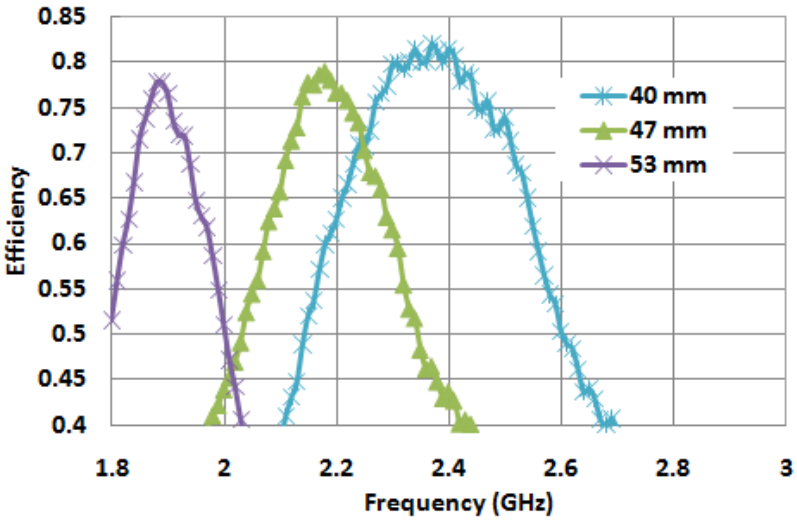

Figure 4-13: Results for the radiation efficiency of the SPA without an isolating layer for various patch side lengths

4.3 Summary

This chapter described the manufacturing process of the SPAs and summarized their experimental measurements. Therefore, the objective 2 was completed. The SPA with an isolating layer has an antenna radiation efficiency of ~80%. When it was elongated, the radiation efficiency drops 5% every 10mm elongation of the SPA with an isolating layer. Later on, after removing the isolating layer inside the SPA, the SPA is keeping functioning with above 78% efficiency after stretching. This radiation efficiency is reasonable compared to commercial metal and dielectric antennas. Therefore, it is ready for the SPA-DEA system.

5: DIELECTRIC ELASTOMER ACTUATOR

5.1 Analysis of the dielectric elastomer actuator

As mentioned in Chapter 1, the dielectric elastomer actuator (DEA) is candidate for mechanically tuning the resonant frequency of an SPA from band to band, because not only it is light-weight, low-cost, easy-to-manufacture, exhibits energy saving characteristics [9]-[18] and can also be fabricated from the same silicone substrate (TC5005). In order to embed the DEA into the SPA-DEA system and optimize the efficiency, understanding the DEA is necessary.

5.1.1 The electrostatic stress of the dielectric elastomer actuator

The DEA works like a DC parallel plate capacitor. Due to an induced electric field, two electrodes with equal but opposite charge are attracted to each other so that they squeeze the elastic dielectric material sandwiched between the electrodes causing the dielectric to latterly expand. Figure 5.1 shows a schematic drawing of the DEA.

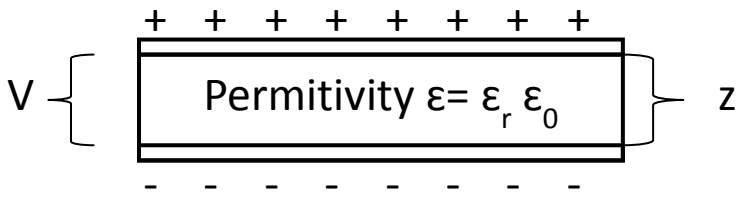

Figure 5-1: The schematic diagram of the cross section of the DEA.

In order to analyze the DEA, we first needed to understand the relation between the activating voltage and the induced electrostatic stress σ_e [9], [11].

If the DEA is activated by a voltage V, the anode of the DEA will have a charge, Q. The work of the DEA is given by

$$w = \int_0^V Q dv \tag{5.1}$$

solving $C = \frac{Q}{V}$ for Q and inserting into (5.1) we obtain

$$w = \int_0^V CV dv = \frac{1}{2} CV^2 \tag{5.2}$$

We also know that $$C = \frac{\varepsilon_r \varepsilon_0 A}{z}, \tag{5.3}$$

where $\boldsymbol{\varepsilon_r}$ is the relative permittivity of the dielectric material, $\boldsymbol{\varepsilon_0}$ is the permittivity of vacuum, *A* is the area of the anode, and *z* is the thickness of the dielectric.

If we substitute (5.3) into (5.2), we obtain

$$w = \frac{\varepsilon_r \varepsilon_0 A}{2z} V^2 \tag{5.4}$$

The change of stored energy is given by taking the derivative of (5.4)

$$dw = \frac{\varepsilon_r \varepsilon_0}{2z} V^2 dA - \frac{\varepsilon_r \varepsilon_0 A}{2z^2} V^2 dz \tag{5.5}$$

Under the assumption that the dielectric material is an incompressible material [13] *Az* is considered to be a constant, and we have

$$dA = -\frac{A}{z} dz$$

dA can be replaced by *dz* in (5.5), and we obtain

$$dw = \varepsilon_r \varepsilon_0 A (\frac{V}{z})^2 dz \tag{5.6}$$

The stress on the DEA when it is activated is

$$\sigma_e = -\frac{1}{A} \frac{dw}{dz} \tag{5.7}$$

Substituting (5.7) into (5.6), we obtain

$$\sigma_e = -\varepsilon_r \varepsilon_0 A (\frac{V}{z})^2 \tag{5.8}$$

This equation (5.8) is used to calculate the electrostatic stress of the DEA.

5.1.2 Analytical simulations of the planar dielectric elastomer actuator

In chapter 1, we mentioned that the siliconeTC5005 as the substrate for the DEA is considered in this work as a linear elastomer [18]. Therefore, using Hook's law, the general matrices to calculate the strain of the DEA are

$$\begin{pmatrix} \varepsilon_{xx} \\ \varepsilon_{yy} \\ \varepsilon_{zz} \end{pmatrix} = \begin{pmatrix} 1/E & -\nu/E & -\nu/E \\ -\nu/E & 1/E & -\nu/E \\ -\nu/E & -\nu/E & 1/E \end{pmatrix} \begin{pmatrix} \sigma_{xx} \\ \sigma_{yy} \\ \sigma_{zz} \end{pmatrix} \tag{5.9}$$

In (5.9), the Young's modulus E=47.5 KPa [18] and Poisson's ratio, ν = 0.5. Appendix A explains why the Poisson`s ratio is equal to 0.5. σ_{xx}, σ_{yy}, and σ_{zz} are stresses along the x, y, and z axes; ε_{xx}, ε_{yy}, and ε_{zz} are strains along the x, y, and z axes.

Figure 5-2 is the top view of the planar DEA. In Figure 5-2, the white square represents the dielectric portion of the DEA, and the black square represents the electrode. Due to the symmetric configuration of the actuator as shown in Figure 5-2, it was sufficient to model only a quarter of the DEA. In Figure 5-2, x_0 is the half length of the relaxed DEA along the x axis, and y_0 is the half length of the relaxed DEA along the y axis. In addition, z_0 is the thickness of the DEA. Note that only the dielectric under the electrodes was simulated. The white edges of the dielectric material without electrodes are negligible because, they will not be compressed.

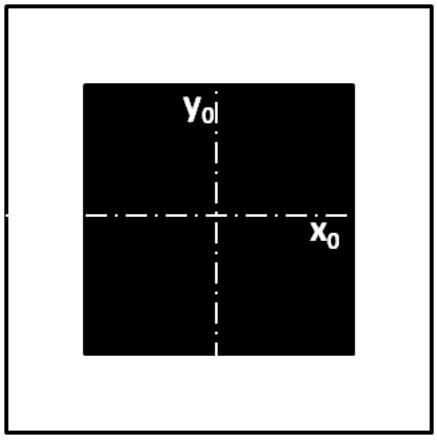

Figure 5-2: The schematic diagram of the planar DEA.

In this analysis, because the pre-strain significantly improved the performance of the DEAs [13], we assumed that the planar DEA was prestretched 100% in the y direction. When the DEA was activated, the electrostatic stress compressed the dielectric along the z-axis, and the DEA only expanded along the x-axis because it was free of constrain in this direction. This procedure transferred the electrical energy to mechanical work. The strain of the DEA along the x-axis was more of a concern because, in the SPA-DEA system, it directly correlates to the deformation of the SPA.

To calculate the displacement of the DEA along the x axis, substituting the boundary conditions of the DEA which was described above in (5.9), we have

$$\begin{pmatrix} \frac{x-x_0}{x_0} \\ 1 \\ \frac{z-z_0}{z_0} \end{pmatrix} = \begin{pmatrix} 1/E & -\nu/E & -\nu/E \\ -\nu/E & 1/E & -\nu/E \\ -\nu/E & -\nu/E & 1/E \end{pmatrix} \begin{pmatrix} 0 \\ \sigma_y \\ -\varepsilon_r \varepsilon_0 (\frac{V}{z})^2 \end{pmatrix} \tag{5.10}$$

where stress σ_{xx} = 0, because there is no any load on this direction, and $\sigma_{zz} = \sigma_e$.

In addition, in (5.10), the half length and the thickness of the activated DEA (*x, z*) are unknown variables, as well as the stress, σ_y, along the y-axis. If we assume x_0=0.04 m, y_0=0.04 m and z_0=0.002 m, the solutions of (5.10) for *x* are around 0.0243 m, and the displacement along the x axis ($\Delta x = |x - x_0| = 0.0157$ m)

5.1.3 An alternative method to simulate the planar dielectric elastomer actuator

Using (5.10), we could calculate the strain and stress of the DEA analytically. However, when the structure is more complicated, as in our case, a finite element analysis is very helpful to the simulation and optimization.

When using finite elements analysis to simulate the planar DEA, a challenge rises because the electrostatic stress function varies with *z*, and it will continue changing unless the system reaches equilibrium. Therefore, although calculating *x* and *z* is easy using (5.10), it requires one or two days to compute using finite element analysis software. Particularly, if we want to add optimization of the SPA-DEA system at the same time, the simulations become very time consuming and, therefore, impractical.

To solve this problem, we determined an algorithm to simplify the function of the electrostatic stress. The pre-strain of the DEA has a significant effect on the performance of the DEA because the pre-strain reduces the thickness of the DEA and increases the electrostatic stress ($\sigma_e = -\varepsilon_r \varepsilon_0 A(\frac{V}{z})^2$). Therefore, two states of the DEA were simulated instead of directly using equation (5.10). These were the pre-strain state of the DEA, and the activated state. In each of these states, the electrostatic stress was constant. Equation (5.11) below is the equation used for the first state:

$$\begin{pmatrix} \frac{x_p - x_0}{x_0} \\ 1 \\ \frac{z_p - z_0}{z_0} \end{pmatrix} = \begin{pmatrix} 1/E & -\nu/E & -\nu/E \\ -\nu/E & 1/E & -\nu/E \\ -\nu/E & -\nu/E & 1/E \end{pmatrix} \begin{pmatrix} 0 \\ \sigma_{yp} \\ -\varepsilon_r \varepsilon_0 (\frac{V}{z_0})^2 \end{pmatrix} \tag{5.11}$$

In (5.11), x_p is half the length of the pre-stretched DEA, z_p is the thickness of the pre-stretched DEA and σ_{yp} is the pre-stress along the y-axis. Substituting the results into (5.12), we obtain the equation for the activated state:

$$\begin{pmatrix} \frac{x_e - x_p}{x_p} \\ 1 \\ \frac{z_e - z_p}{z_p} \end{pmatrix} = \begin{pmatrix} 1/E & -\nu/E & -\nu/E \\ -\nu/E & 1/E & -\nu/E \\ -\nu/E & -\nu/E & 1/E \end{pmatrix} \begin{pmatrix} 0 \\ \sigma_{ye} \\ -\varepsilon_r \varepsilon_0 (\frac{V}{z_p})^2 \end{pmatrix} \quad (5.12)$$

where x_e is the final length of the DEA after activation, z_e is the thickness of the activated DEA and σ_{yp} is the stress along the y-axis after the activation. In those variables, x_e has the same physical definition as the x in (5.10).

Using (5.12), we then calculated $x_e \approx 0.0240$m and $\Delta x = |x_e - x_0| = 0.0160$m. Comparing these results to those results from (5.10) $\Delta x = 0.0157$m, there is only 0.0003 m difference which is a percentage difference is 1.8%. In addition, with the alternative method, we were able to reduce the massive computing time and make the simulation more practical. Later, we applied this method to the analysis of the SPA-DEA system with the finite element method.

5.2 Fabrication of the dielectric elastomer actuator

To fabricate the DEA, we prepared a flat sheet of TC5005 with 1 mm thickness as the dielectric of the DEA. The ratio of A, B, and C components were same as those described in Chapter 3. Then, we used a screen-printing method to paint two electrodes on the DEA and this process is described below. Notice that the process is a schematic description. The scale bar is not shown in

following pictures, because the size of the DEA is changing depending on its application.

First, we placed two thin PE sheets as masks to cover the top and bottom of the TC5005 sheet (Figure 5-3a) and in the middle of the masks, there were windows for painting electrodes. Secondly (the size of this window can be adjusted depending on applications), we used a pipette to deposit the carbon powder (Vulcan Xc-72R) on the dielectric (Figure 5-3b). Next, the carbon powder was spread out until the exposed dielectric was fully covered (Figure 5-3c and 5-3d). This process was repeated on the other side to prepare two electrodes on the DEA. Finally, we used plastic clamps and screws to constrain the DEA for the pre-stretching, and two conductive strips made from copper were extended out for connecting to a voltage amplifier (EMCO Q101) [34] (Figure 5-3e).

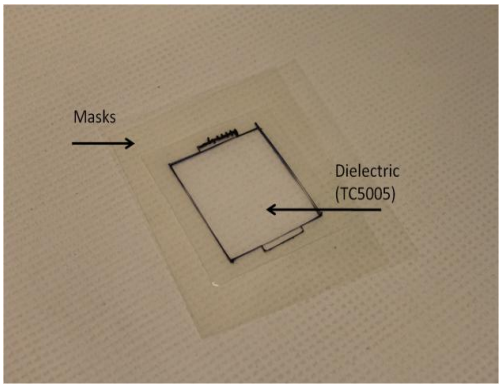

(a)The TC5005 covered by masks

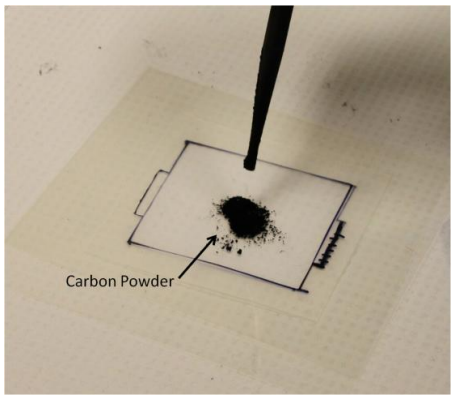

(b) Deposit the carbon powder

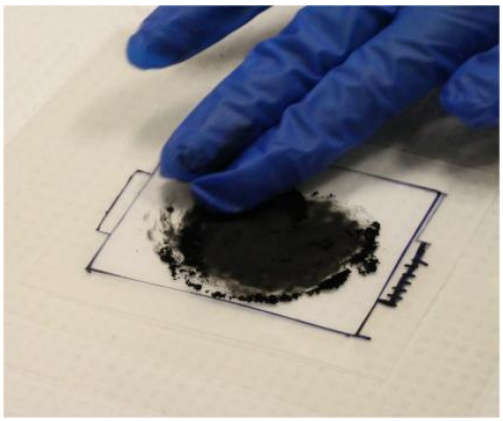

(c) Spread out the carbon powder

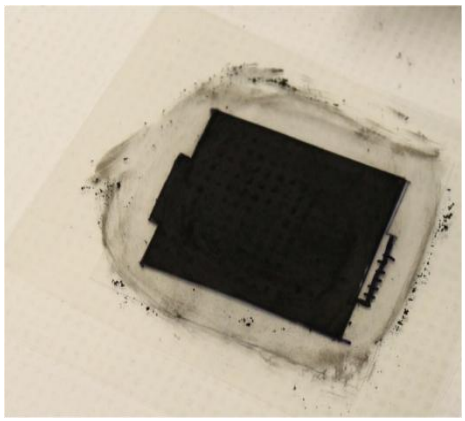

(d) Repeat the third step on the other side

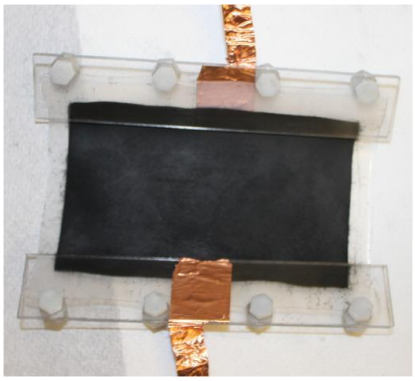

(e) Constrained by plastic clamps

Figure 5-3: Fabrication steps of the DEA.

5.3 Summary

In this chapter, we introduced an analytical analysis of the simple planar DEA. The method can be used to decrease computing time, and it was applied to further simulations of the SPA-DEA system. Finally, by fabricating the DEA, the third objective was achieved.

6: FINITE ELEMENT ANALYSIS OF THE STRETCHABLE PATCH ANTENNA SYSTEM USING DIELECTRIC ELASTOMER ACTUATOR

6.1 Finite element model

In the proposed configuration discussed in Chapter 3, the DEA is used to control the side length of the SPA. It is desirable to design the DEA such that its size is minimized to obtain an overall compact system. Note that the effective DEA deformations are highly influenced by the amount of initial pre-stretching and imposed boundary constraints. A finite element model of the system was, therefore, developed to investigate the effect of these parameters. As in Chapter 5, the DEA was considered to be a linear isotropic material and this assumption served to minimize the simulation time during the optimization process.

Due to the symmetric configuration of the actuator, only a quarter of the DEA model was simulated, as shown in Figure 6-1. In Figure 6-1a, x_0 is half the length of the relaxed DEA along the x axis, and y_0 is half the length of the relaxed DEA along the y axis; y_c is defined as half the length of the interface between the DEA and the un-stretchable material; x_p and y_p are the dimensions of the DEA after mechanical pre-stretching, achieved by pre-tensioning the un-stretchable cloth in the x direction (Figure 6-1a) and deforming the DEA in the y direction through mechanical constraints (Figure 6-1b). Upon electrical activation, the DEA expanded in the x direction and its new length in the x direction was defined as x_e. The displacement caused by activation was defined as $\Delta x=|x_e-x_p|$. Note that

no displacements due to electrical activation were observed in the y direction as the DEA was constrained along the y-axis. Figure 6-1b schematically summarizes the different configurations assumed by the DEA and the variables used in our analysis.

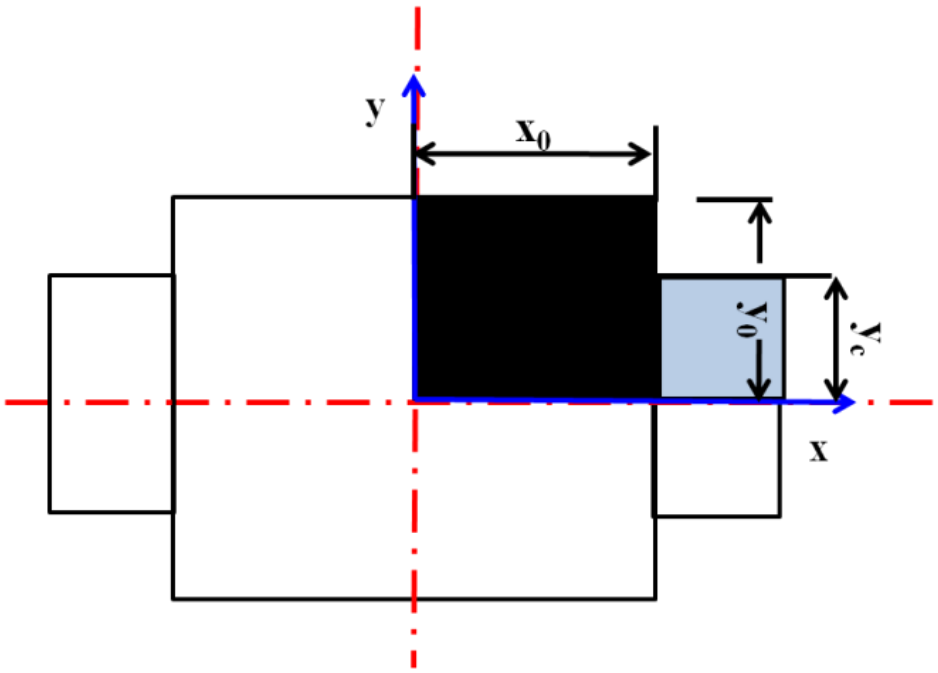

(a)

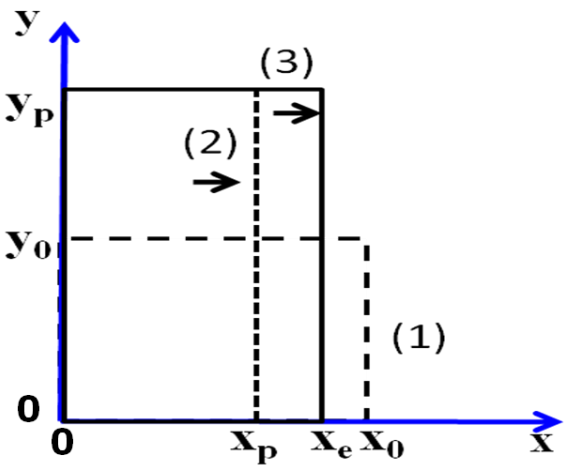

(b)

Figure 6-1: (a) Schematic diagram of the DEA; (b) Parameters used to describe the three DEA states, namely (1) relaxed, (2) mechanically pre-stretched, and (3) electrically activated.

The design parameters were explored through simulations performed using the finite element method (FEM) software COMSOL 4.1. A script written in MATLAB was used to automatically initiate each FEM simulation and automatically post-process the results. Figure 6-2 shows the flow chart for the simulations. The method we applied for these simulations is the alternative method introduced in Chapter 5 (see section 5.1.3).

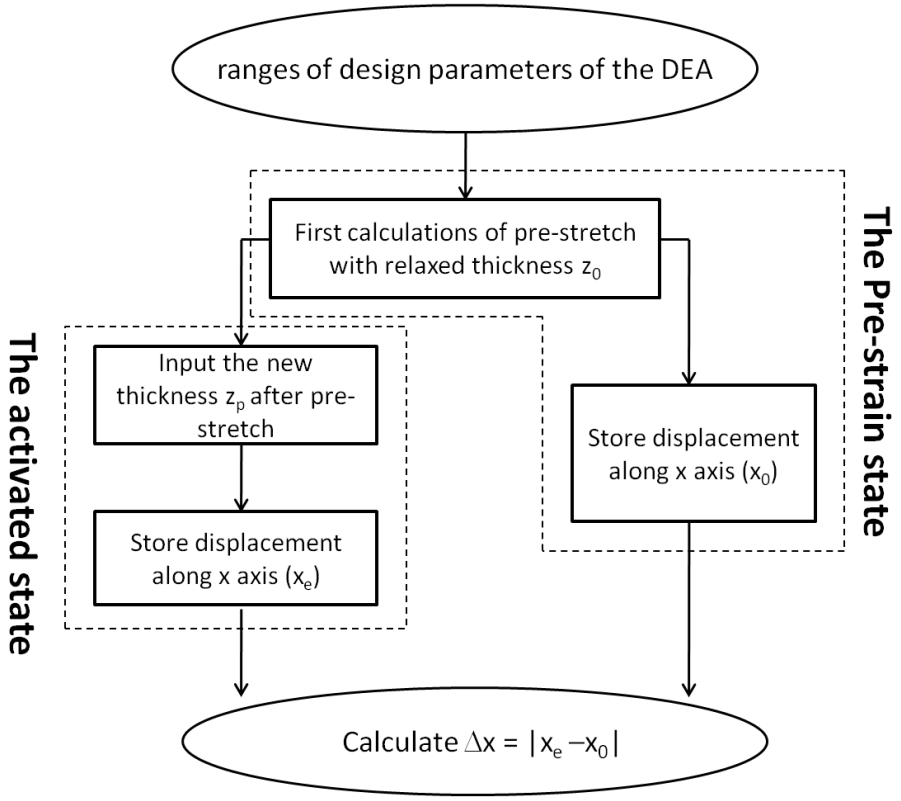

Figure 6-2: The algorithm diagram for simulations.

As seen in Figure 6-2, the simulation was divided into two steps, denoted by the dashed lined boxes. The first batch of calculations simulated the pre-strain of the DEA, otherwise called the pre-strain state. Then, the second batch of

calculations simulates the activated DEA, which is referred to as the activated state. Finally, we calculated the displacement caused by activation, Δx, which causes the deformation of the SPA. Because we only need to realize a limited deformation range (40 mm–53 mm) to fulfill design requirements as mentioned in section 3.2, the Δx is one of the references for optimizing the implement efficiency. Simulations of larger or smaller displacements along the x axis are not necessary for our SPA-DEA system.

6.2 Optimizing the dielectric elastomer actuator for the stretchable patch antenna system

For the DEA in its relaxed state, six design parameters were identified: x_0 and y_0, the width of the cloth, y_c, the percentage strains S_x and S_y defined as $S_x = |x_p\text{-}x_0|/x_0$ and $S_y = |y_p\text{-}y_0|/y_0$ respectively, and the electric field, E, applied to the DEA's electrodes to electrically activate the actuator. Table 5-1 summarizes the range and step size used to investigate the workspace described by these six parameters. All of the elements of the analyzed 3D actuation system were modelled with 4052 tetrahedral elements. Meanwhile, 2908 2D triangular elements were also modelled for the interactive boundary surface between DEA and the inextensible cloth.

Table 6-1: Range and step size of the FEM parameters

Parameter	x_0 **(m)**	y_0 **(m)**	y_c **(m)**	$S_x = \lvert x_p - x_0 \rvert / x_0$	$S_y = \lvert y_p - y_0 \rvert / y_0$	E **(V/µm)**
Range	[0.01,0.1]	[0.01,0.1]	[0.01,0.03]	[0%,25%]	[0%,106%]	[0,10]
Step Size	0.01	0.01	0.005	0.8%	15%	0.2

Figure 6-3 summarizes the results obtained. The percentile displacement Δx (obtained for E = 10V/mm) exponentially increases with pre-straining in the x and the y directions. The highest admissible values of S_x and S_y were, therefore, selected for developing the setup of the model. Strains in the x and the y directions (Figure 6-1b) were, respectively, limited to S_x = 25% and S_y = 100% in order to minimize the risk of mechanical failure of the actuator and assure reliable behavior over a large number of cycles. These two values guaranteed an equal average stress distribution in the proximity of the constraints in the x and the y directions. The length of the constraints in x and y, namely x_0 and y_c, was unequal, as discussed below.

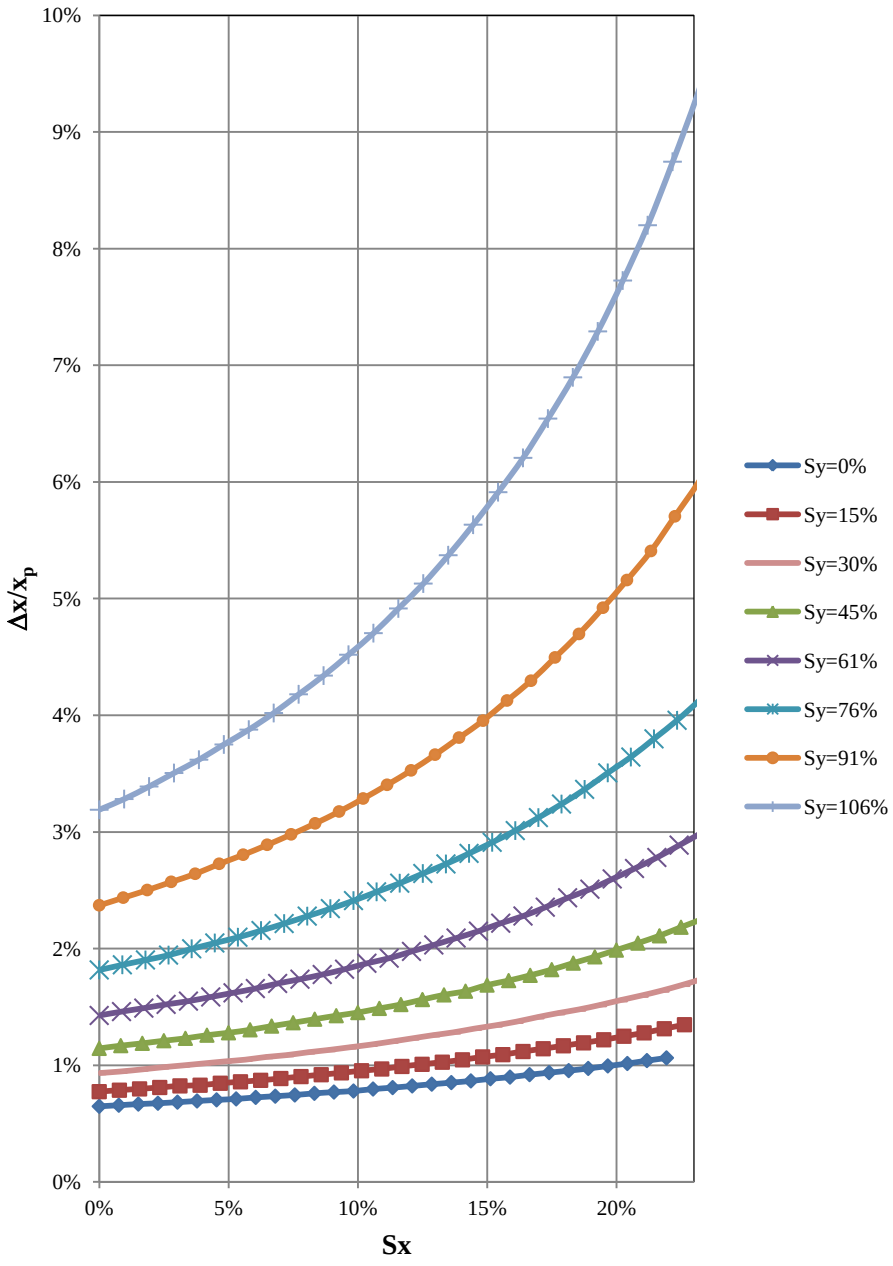

Figure 6-3: $\Delta x/x_p$ of the x component pre-strain of the DEA (*E*=10V/μm).

Results shown in Figure 6-3 were obtained for a fixed ratio C = y_c/y_0 equal to 30%, the optimal value within the geometrical constrains imposed in this

thesis. Figure 6-4 shows the relationship between C and the percentile displacement Δx, where $\Delta x/x_p$ increases when C decreases. We limited the lower bound to 30% as smaller values would have complicated the fabrication of a prototype and would have increased the stress concentration at the interface between the DEA and un-stretchable cloth.

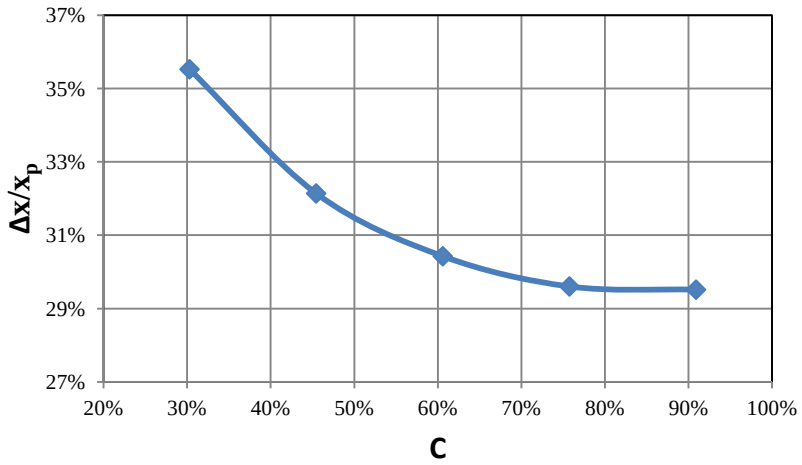

Figure 6-4: $\Delta x/x_p$ to C (S_x = 25%, S_y = 100%, E = 10V/μm).

In order to minimize the dimensions of the actuation system, the DEA was designed to be the smallest dimensions that still enabled it to achieve the maximum deformation of the antenna. In this case, the deformation of the antenna ranged from 40 mm to 53 mm (Section 3.2), corresponding to a displacement of 13mm (Δx = 6.5 mm) and a strain of 35% in the x direction. Figure 6-5a shows the displacement along the x-axis for different DEA sizes, namely for different pre-stretched DEA areas $A_p = x_p y_p$. This plot was obtained for the identified parameters S_x = 25%, S_y = 100%, C = 30%. Multiple curves,

corresponding to different values of x_0, are shown in this figure. Figure 6-5b, which presents a close-up view, shows that for a maximum displacement of 6.5 mm, the curve obtained for x_0=4 cm provided the smallest pre-stretched area (1.7 cm^2). The final size of the actuator was therefore, determined to be 8 cm × 6 cm in its relaxed state.

Note that a pre-strain in the x direction of the actuator yields a pre-strain on the antenna (Figure 3-1). The antenna was, therefore, designed to be 32 mm long in its un-stretched configuration in order to be able to operate within the 40 mm-53 mm range once connected to the actuation system.

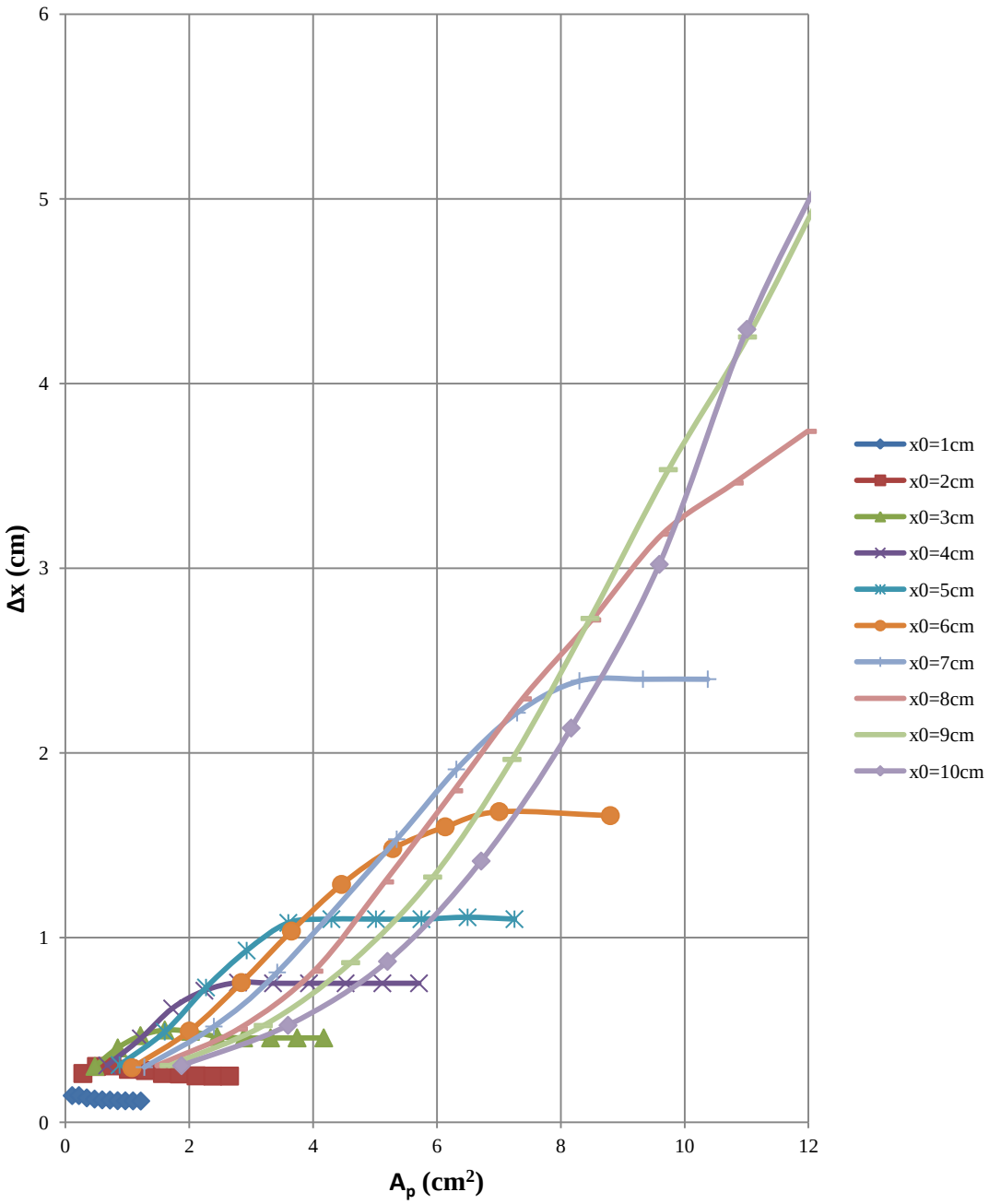
6
5
4
3
2
1
0
Δx (cm)
0
2
4
6
8
10
12
Ap (cm2)
x0=1cm
x0=2cm
x0=3cm
x0=4cm
x0=5cm
x0=6cm
x0=7cm
x0=8cm
x0=9cm
x0=10cm

(a)

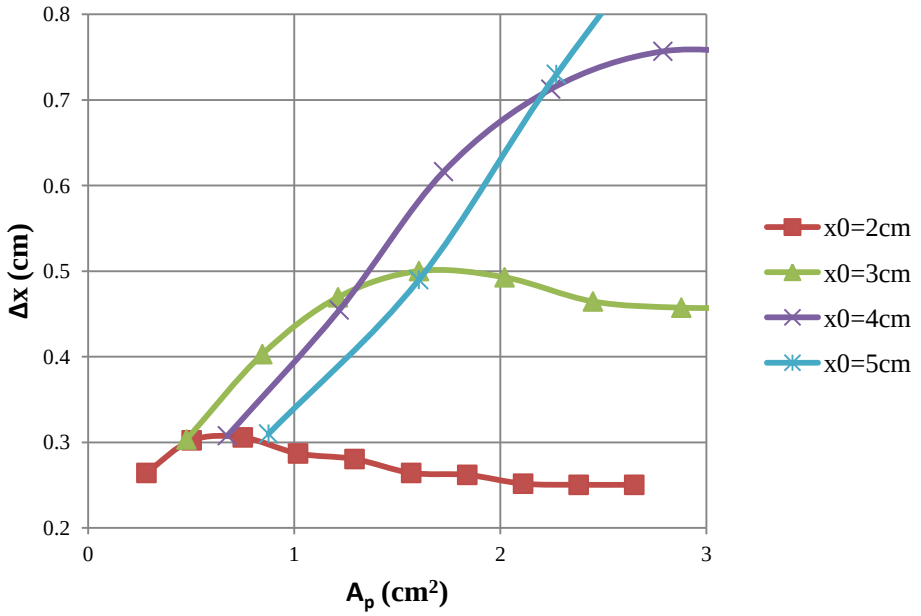

(b)

Figure 6-5: Displacement of the x axis versus prestretched DEA Area (A_p). (a) Zoomed out view; (b) Zoomed in view highlighting the requested maximum deformation the DEA should provide. (S_x = 25%, S_y = 100%, *E* = 10V/µm, C = 30%).

In addition, the simulations of the DEA were not only useful to investigate this SPA-DEA system. In fact, in order to find out the optimal design parameters for this particular application, many sizes of the DEA have been simulated (Figure 6-5). Therefore, in future, if another deformation of the DEA is requested, the figure 6-5 could be a reference data.

6.3 Comparison of the experimental results and simulations

With the design parameters determined by FEM, the DEA was electrically activated, and deformations of the patch antenna were measured by post processing snapshots from a measurement imaging system software, ImageJ. Figure 6-6 shows the strain along the x axis of the patch antenna (ε_a) for different values of the electrical field. The average of differences between the simulation results and the experimental data was 3%.

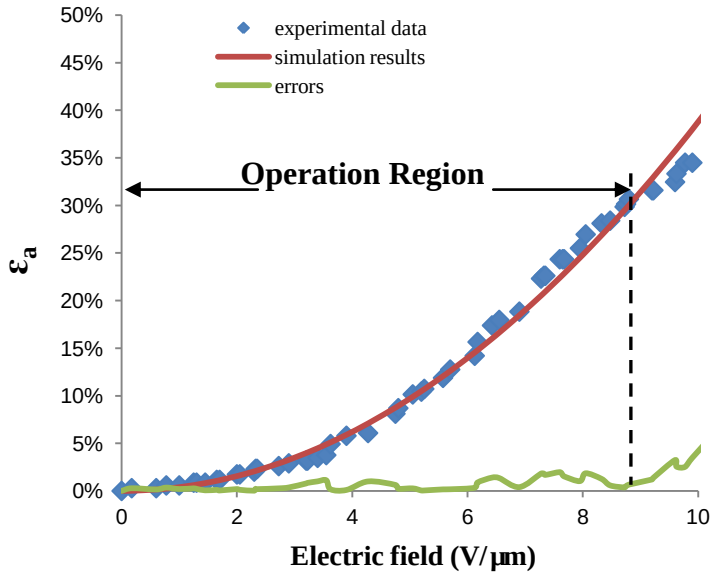

Figure 6-6: Strain of the patch antenna along the x axis for different values of the imposed electric field.

The resonant frequency and efficiency of the antenna was measured as before by Dr. Mazlouman. The input port voltage reflection coefficient, $S_{11,}$ of the antenna (including the complete system) was measured using a Vector Network

Analyzer (VNA). Figure 6-7 depicts the variation of the resonance frequency of the antenna by varying the patch side length.

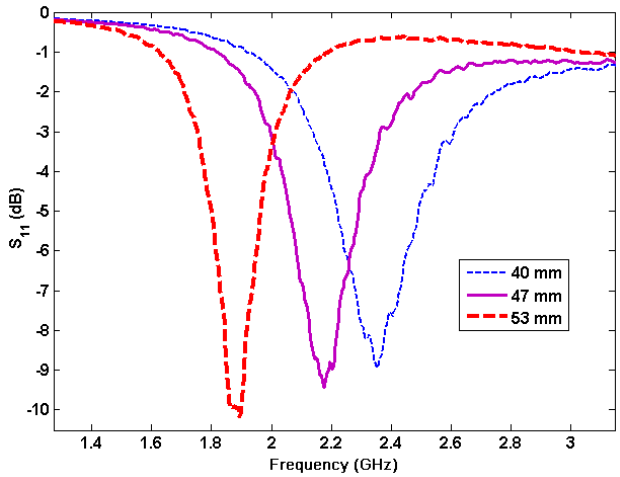

Figure 6-7: Variations of the measured S_{11} of the antenna system for various patch side lengths that can be attained using the DEA small belt system.

6.4 Summary

FEM was used to calculate the optimal design parameters and a prototype was fabricated and analyzed. Moreover, the experimental measurements agreed with simulation results calculated by the same FEM within 3% difference. The objective 4 to optimize mechanical design of the SPA-DEA configuration has been accomplished. The size of the relaxed DEA should be 8 cm ×6 cm. Meanwhile, the experimental measurements demonstrated that the performance of the SPA-DEA system is capable of producing the required design.

7: THE PROTOTYPE OF THE STRETCHABLE PATCH ANTENNA SYSTEM USING DIELECTRIC ELASTOMER ACTUATOR

7.1 The first prototype of the stretchable patch antenna system using dielectric elastomer actuator

A prototype, configured, as schematically represented in Figure 3-1, was developed. The dimensions of both the patch antenna and the actuation system were selected based on the previously presented analyses in section 6.2.

The planar DEA used in the SPA-DEA system was manufactured following the procedure first introduced in section 5.2. As mentioned previously, electrodes were created by embedding carbon particles on the surface of the silicone substrate. The DEA was then electrically activated using a voltage amplifier (EMCO Q101), which provided 0.5-Watt maximum power input [34]. The assembled prototype is shown in Figure 7-1.

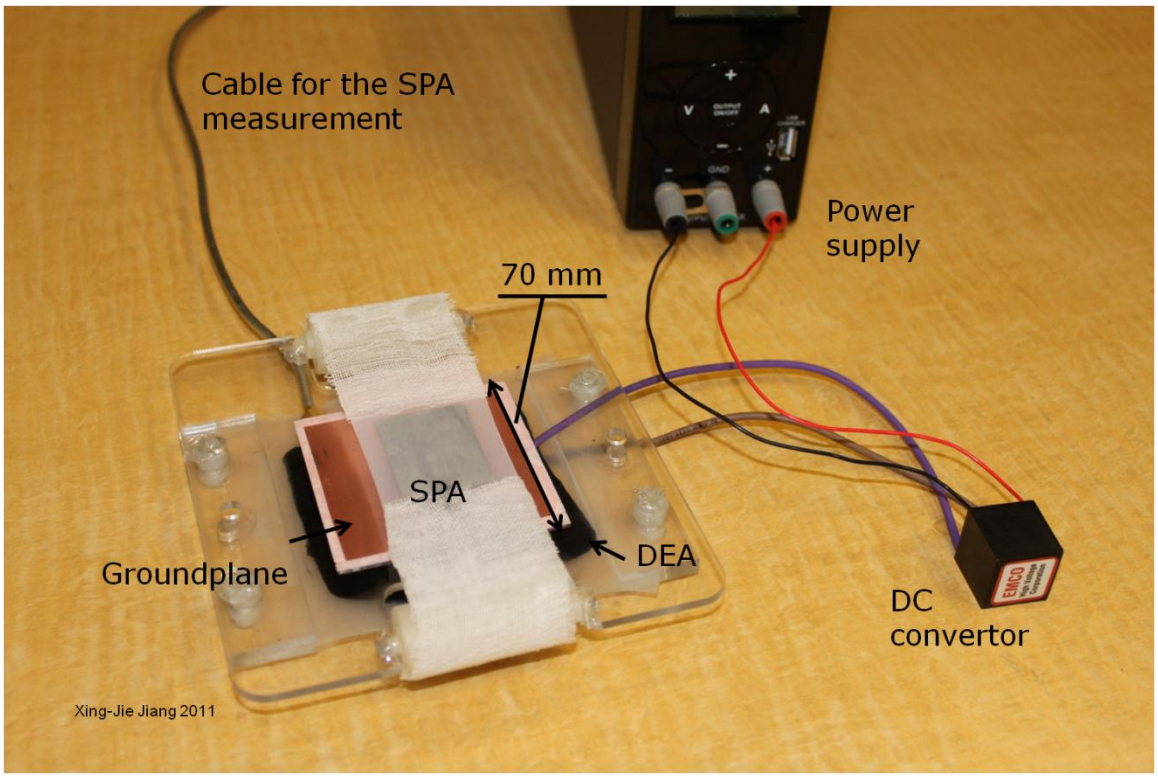

Figure 7-1: The first prototype of the SPA-DEA system

The transparent framework was fabricated from 2 mm thick PMMA, and it was cut into shape using the 60-watt CO_2 laser cutter (VersaLASER® VLS3.60, 60W Laser Cartridge). PMMA was used as a supporting structure for three reasons: first, it is good insulator from electricity. Second, PMMA is much lighter than a cooper plate of the same volume and third, it is transparent, so it is easy to observe working conditions on both sides without physically disturbing the sample.

The copper groundplane was placed in the middle of the PMMA structure and two edges of the planar PMMA structure were each attached a single wheel.

The belt connecting the SPA and DEA was stretched over the wheels so that the belt could move smoothly by simply rolling the two wheels. In addition, to being pre-stretched by the SPA, the DEA was also stretched and constrained perpendicularly.

7.2 The compacted prototype of the stretchable patch antenna system using dielectric elastomer actuator

Upon reviewing our design, it was determined that several components of the prototype were not necessary. In order to make the entire SPA-DEA system more compact and lighter, the size of the PMMA structure were reduced and the clamps used to constrain the DEA were removed. Finally, a more compact prototype was manufactured as shown in Figure 7-2. Although it was more difficult to manufacture the compact prototype than the first one the final prototype will be more easily integrated with other equipment.

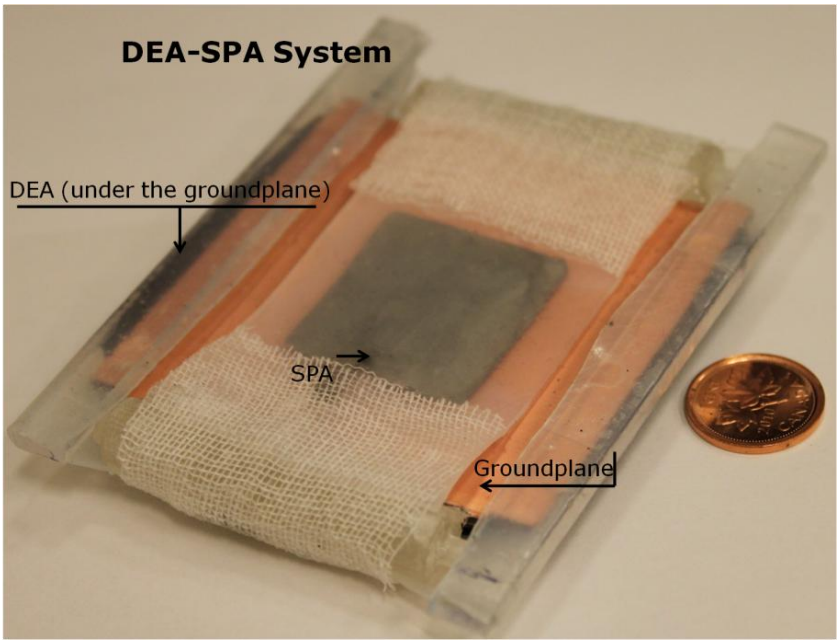

Figure 7-2: The final prototype of SPA-DEA system

7.3 Summary

The objective 5 was achieved in this chapter. Two prototypes of the SPA-DEA system were fabricated and shown in this chapter. While the first prototype was easier to assemble, the second prototype reduced the amount of necessary materials and became more compact and lighter.

8: CONCLUSION AND FUTURE WORK

8.1 Conclusion

During this study, the five objectives mentioned in Chapter 1 have been accomplished.

Objective 1: Propose an innovative SPA-DEA configuration

In this thesis, an innovative SPA-DEA configuration was proposed as a solution to enable wireless communication. The variation of the side length of the SPA was determined from 40 mm to 53mm in order to switch the resonant frequency of the SPA between bands. In addition, the size of the groundplane was selected as 70 mm × 70 mm.

Objective 2: Propose and test a manufacturing procedure to fabricate an SPA.

A stretchable patch antenna with an isolating layer was successfully manufactured firstly. The SPA with an isolating layer has 80% radiation efficiency at its relaxed state, but its radiation efficiency dropped 5% when the SPA was extended every 10 mm. Because the isolating layer was considered as the possible cause of this problem, a manufacturing procedure of the SPA without an isolating layer was developed. As expected, the radiation efficiency of the SPA without an isolating layer stayed above 78%. The SPA without an isolating layer was used in the SPA-DEA system.

Objective 3: Fabricate a DEA

A DEA design was selected and fabricated for actuating the SPA with the goals of keeping the system both lightweight and flexible. Section 5.2 demonstrated the fabrication process of the DEA.

Objective 4: Optimize the mechanical design of the SPA-DEA configuration

To minimize the size of the DEA and to obtain a compact system, the design parameters of the DEA were simulated and optimized. The final size of the DEA was 80 mm × 60mm.

Objective 5: Characterise the performance of the SPA-DEA system

The SPA-DEA system was tested and measured. The deformation of the SPA agreed with the simulation results from the same FEM within 3% difference. The final prototype is demonstrated and results are in Figure 7-2.

8.2 Future work

The rigid copper groundplane is the only rigid part of the SPA-DEA system. To make the SPA-DEA system 100% flexible, the groundplane should be modified and some materials with stiffness between that of PMMA and TC5005 could be considered as a groundplane materials.

APPENDIX A

This appendix mathematically explained the reason why the poisson ratio, ν, of TC5005 is 0.5.

Firstly, assume there is a material that has a unit volume where $x_0 = y_0 = z_0 = 1$. If we apply a stress along the x-axis, there is a corresponding strain ε. In this case, x becomes $x = \varepsilon+1$, $y = z = 1-\nu\varepsilon$, where ν is Poisson ratio.

Therefore, the final volume of this material (v_f) becomes

$$v_f = x \cdot y \cdot z = (\varepsilon+1)(1-\nu\varepsilon)$$

$$= (\varepsilon+1) (1-2\nu\varepsilon+\nu^2\varepsilon^2)$$

$$=(1-2\nu\varepsilon+\nu^2\varepsilon^2+\varepsilon-2\nu\varepsilon^2+\nu 2\varepsilon^3)$$

The change in volume is given by

$$\delta v = v_f - v_0 = -2\nu\varepsilon+\nu^2\varepsilon^2+\varepsilon-2\nu\varepsilon^2+\nu 2\varepsilon^3$$

Furthermore, if we consider the strain, ε, to be small, ε^2 and ε^3 are close to zero and we have

$$\delta v/v = \varepsilon (1-2\nu)$$

From the above equation, If assume that the volume of the TC5005 is a constant, Poisson ratio has to be equal to 0.5.

REFERENCE LIST

[1] D. Graham-Rowe, "http://www.technologyreview.com/biomedicine/24889/page1&2", Mar. 2010

[2] J. T. Bernhard, *Reconfigurable antennas,* Morgan & Claypool Publishers, 2007

[3] H.-J. Kim, C. W. Son, and B. Ziaie, "A multiaxial stretchable interconnect using liquid-alloy-filled elastomeric microchannels", *Appl. Phys. Lett.*, vol. 92, no. 1, pp. 011904-1–3, Jan. 2008.

[4] H.-J. Kim, M. Zhang, and B. Ziaie, "A biaxially stretchable interconnect with liquid alloy joints on flexible substrate", in *Proc. Transducers'07 and Eurosensors XXI. 14th Int. Conf. on Solid-State Sensors, Actuators and Microsyst.*, Jun. 2007, pp. 1597–1600.

[5] H.-J. Kim, C. W. Son, and B. Ziaie, "Multi-axial super-stretchable interconnects with active electronics", in *Proc. IEEE-MEMS'08 Int. Conf.*, Jan. 2008, pp. 828–831.

[6] J-H So, J. Thelen, A. Qusba, G. J. Hayes, G. Lazzi, and M. D. Dickey, "Reversibly Deformable and Mechanically Tunable Fluidic Antennas", *Adv. Funct. Mater.* 2009, 19, 3632-3637.

[7] S. Cheng, Z. Wu, P. HallbJorner, K. Hjort, and A. Rydberg, "Foldable and Stretchable Liquid Metal Planar Inverted Cone Antenna", *IEEE Transactions on Antennas and Propagation*, Vol. 57, No. 12, Dec. 2009.

[8] S. J. Mazlouman, X. Jiang, A. Mahanfar, C. Menon, and R. G. Vaughan, "*A Reconfigurable Patch Antenna using Liquid Metal Embedded in a Silicone Substrate*", *IEEE Transactions on Antennas and Propagation*. Doi:10.1109/TAP.2011.2165501

[9] R. E. Pelrine, R. D. Kornbluh, J. P. Joseph, "Electrostriction of polymer dielectrics with compliant electrodes as a means of actuation", *Sens. Actuators A*, 1998, 64, 77.

[10] G. Kofod, "Dielectric Elastomer Actuators", *Ph.D. Thesis*, Technical University of Denmark, Sept. 2001.

[11] F. Carpi, P. Chiarelli, A. Mazzoldi, D. De Rossi, “Electromechanical characterisation of dielectric elastomer planar actuators: comparative evaluation of different electrode materials and different counterloads”, *Sens. Actuators A,* 2003, 107, 85.

[12] F. Carpi, A. Mazzoldi, D. De Rossi, “High-strain dielectric elastomer for actuation”, *Proc. SPIE 2003*, 5051, 419.

[13] C. M. Hackl, H-Y Tang, R. D. Lorenz, L-S Turng, and D. Schröder, “A multidomain model of planar electro-active polymer actuators”, *IEEE Trans. on Industry Applications*, Vol. 41, No. 5, Sept./Oct. 2005, 1142-1148.

[14] G. Kofod, M. Paajanen, S. Bauer, “New design concept for dielectric elastomer actuators”,*Proc. SPIE 2006*, 6168, 61682J.

[15] Q. Pei, M. Rosenthal, S. Stanford, H. Prahlad, R. Pelrine, “Interpenetrating Polymer Networks for High-Performance Electroelastomer Artificial Muscles”, *Smart Mater. Struct. 2004*, 13, N86.

[16] F. Carpi, D. De Rossi, “Contractile folded dielectric elastomer actuators”, *Proc. SPIE 2007*, 6524, 65240D.

[17] R. Pelrine, R. Kornbluh, Q. Pei, S. Stanford, S. Oh, J. Eckerle, “Dielectric Elastomer Artificial Muscle Actuators: Toward Biomimetic Motion”, *Proc. SPIE 2002*, 4695, 126.

[18] M. Soleimani and C. Menon, “Preliminary investigation of a balloon-shape actuator based on electroactive elastomers”, *Smart Mater. Struct.* 19 (2010) 047001.

[19] S. Cheng, A. Rydberg, K. Hjort, and Z. Wu, “Liquid metal stretchable unbalanced loop antenna,” *Applied Physics Letters*, Vol.94, No.14, pp.144103-144103-3, Apr 2009.

[20] M. Kubo, X. Li, C. Kim, M. Hashimoto, B. J. Wiley, D. Ham, and G. M. Whitesides, “Stretchable Microfluidic Radiofrequency Antennas,” *Advanced Materials*, Vol. 22, pp. 2749–2752, 2010.

[21] D. M. Pozar, “Microstrip antenna aperture-coupled to a microstripline,” *Electron. Lett.*, Vol. 21, No. 2, pp. 49-50, Jan. 1985.

[22] P. Sullivan, and D. Schaubert, “Analysis of an aperture coupled microstrip antenna,” *IEEE Trans. Antennas and Propagation*, Vol.34, No. 8, pp. 977- 984, Aug 1986.

[23] Sylgard 184 Silicone Elastomer datasheet, ww.dowcorning.com.

[24] TC 5005 A/B-C datasheet, BJB Enterprises, www.bjbenterprises.com.

[25] R. Pelrine, R. Kornbluh, J. Joseph, R. Heydt, Q. Pei, S. Chiba, “High-field electrostriction of elastomeric dielectrics for actuators”, Mater. Sci. Eng. C 2000, 11, 89.

[26] W. C. Roentgen, ‘‘About the Changes in Shape and Volume of Dielectrics Caused by Electricity’’, *ser. Annual Physics and Chemistry Series*, Vol. 11, sec III, G. Wiedemann, Eds., J. A. Barth Leipzig, Germany 1880, p. 771 German.

[27] R. Kornbluh, R. Pelrine, Q. Pei, R. Heydt, S. Stanford, S. Oh, J. Eckerle, “Electroelastomers: Applications of Dielectric Elastomer Transducers for Actuation, Generation and Smart Structures”, *Proc. SPIE 2002*, 4698, 254.

[28] R. Kornbluh, R. Pelrine, Q. Pei, S. Oh, J. Joseph, ”Ultrahigh Strain Response of Field-Actuated Elastomeric Polymers”, *Proc. SPIE 2000*, 3987, 51.

[29] Report: *Final Acts of the WARC for Dealing with Frequency Allocation in Certain Parts of the Spectrum* (WARC-92), Article 2701, PP:280, ISBN: 92-61-04661-4.

[30] TC 5005 A datasheet, BJB Enterprises, www.bjbenterprises.com.

[31] TC 5005 B datasheet, BJB Enterprises, www.bjbenterprises.com.

[32] TC 5005 C datasheet, BJB Enterprises, www.bjbenterprises.com.

[33] http://www.microwavecookingforone.com/Glad/GladPlasticWraps.html

[34] EMCO Q series datasheet, http://www.emcohighvoltage.com/pdfs/qseries.pdf